Investigating *Pseudo-nitzschia australis* introduction to the Gulf of Maine with observations and models

Suzanna Clark ^{a*}, Katherine A. Hubbard ^b, Dennis J. McGillicuddy, Jr. ^c, David K. Ralston ^c, Sugandha Shankar ^b

^a MIT/WHOI Joint Program in Oceanography/Applied Ocean Sciences and Engineering 86 Water St. Woods Hole, MA, 02543, USA

^{*} Corresponding author: sclark@whoi.edu

^b Florida Fish and Wildlife Conservation Commission-Fish and Wildlife Research Institute, 100 8th Ave SE, St. Petersburg, FL, 33701, USA

^c Woods Hole Oceanographic Institution 86 Water St. Woods Hole, MA, 02543, USA

1 1 Introduction

28

2 The harmful algal genus *Pseudo-nitzschia* is a lightly silicified diatom of growing global presence 3 and increasing concern (Bates et al., 2018; Trainer et al., 2012). Species of the genus are often 4 described as "cosmopolitan" because they can persist in a wide range of temperature conditions 5 (Hasle, 2002), and because their distributions span estuaries, coastal environments, and the open 6 ocean (Bates et al., 2018). Some *Pseudo-nitzschia* species produce domoic acid (DA), a neurotoxin 7 responsible for Amnesic Shellfish Poisoning. More than 52 Pseudo-nitzschia species have been 8 identified worldwide, and at least half are confirmed DA producers (Bates et al., 2018). 9 In 2016 in the Gulf of Maine (GOM), DA concentrations exceeded the regulatory limit of 20 μg 10 DA g^{-1} of shellfish tissue, leading to the first regional DA-induced shellfishery closures (Bates et 11 al., 2018; Clark et al., 2019; Hubbard et al., 2017; Lewis et al., 2017). The bloom began in the Bay 12 of Fundy in late September, 2016, and progressed along the coast of Maine, continuing into the 13 second week of October. Fourteen Pseudo-nitzschia species had been identified in the region 14 prior to the DA event (Fernandes et al., 2014), but the record DA concentrations were caused 15 primarily by the novel appearance of *P. australis* (Bates et al., 2018; Clark et al., 2019). 16 In observations from the 2016 DA event, neither cell concentrations nor relative species 17 abundance correlated strongly with various environmental parameters (temperature, salinity, 18 nitrate, ammonium, silicic acid, phosphate, or nutrient ratios). In addition, except for salinity, 19 environmental parameters were not significantly different in 2016 compared to previous years 20 (2012-2015) (Clark et al., 2019). Salinity was significantly higher in 2016 compared to the four 21 previous years (0.4-1.5 PSU greater), but the salinity difference was not enough to result in 22 improved growth conditions based on the literature for P. australis (Doucette et al., 2008; 23 Thessen et al., 2005). Clark et al. argued that, because of the similarities in environmental 24 parameters across the study period, it was unlikely that P. australis was able to bloom because 25 of a sudden favorable change in conditions. Moreover, P. australis was not detected in the region prior to 2016 in either microscopy or genetic analysis. 26 An alternative explanation to changing environmental conditions for the novel bloom in 2016 is 27

that P. australis was introduced to the region in a process linked to the anomalously saline

conditions in the GOM (Clark et al., 2019). Of the primary source waters flowing into the GOM, Gulf Stream Ring water (GSRW) is saltier than Slope Water or Scotian Shelf Water (Townsend et al., 2015). Previous studies have shown that GSRW can contribute to or modify Northeast Channel inflows (Brooks, 1987), and measurements at the Northeast Regional Association of Coastal Ocean Observing Systems (NERACOOS) Buoy M suggested the presence of GSRW in the GOM interior in July 2013 (Townsend et al., 2015) and again in July 2016 (Clark et al., 2019). GSRW is not the only potential source for anomalously saline water, however. From 1990 to 2015, Brickman et al. (2018) observed near-bottom anomalies upstream on the Scotian Shelf that alternate between warm and saline or fresh and cool. With a model they showed that such anomalies form due to interactions between the Gulf Stream and Labrador Current off of the Grand Banks in the North Atlantic Ocean, propagate toward the southwest, and penetrate into the GOM via the Northeast Channel. Based on both observations and model results, Brickman et al. argued that warm/saline anomalies increased in frequency and magnitude from 2006 to 2015. The correspondence of *P. australis* and an anomalous water mass is not without precedence. In 2015, a P. australis bloom on the West Coast of the United States led to record-breaking DA concentrations in Monterey Bay, CA (Ryan et al., 2017). The bloom occurred during the North Pacific Ocean Warm Anomaly, during which sea surface temperatures were more than 2.5°C higher than the long-term average (McCabe et al., 2016). The anomalously warm water is thought to have contributed to the bloom, either as a primary factor (McCabe et al., 2016) or as a contributing factor along with intermittent upwelling of waters with an anomalously low silicato-nitrate ratio (Ryan et al., 2017). Thus, the anomalies observed in recent years in the GOM region (increased salinity along the coast of Maine and in Jordan Basin (Clark et al. 2019), and warm, saline anomalies on the Scotian Shelf (Brickman et al. 2018)) may relate to the introduction of P. australis. This paper uses field data, a hydrodynamic model, and a Lagrangian particle tracking model to

29

30

31

32

33

34

35

36

37

38

39

40

41

42

43

44

45

46

47

48

49

50

51

52

53

54

55

address the following questions:

• What are the most likely sources of *P. australis* to the Gulf of Maine?

- Was the connectivity from potential source regions to the Gulf of Maine different in 2016
 compared to previous and subsequent years?
 - Do model results indicate differences in hydrographic conditions in the Gulf of Maine that may have affected *P. australis* bloom timing, location, or distribution?

The following sections describe the study site, field data, hydrodynamic model, and particle tracking model and analysis. Simulations of the hydrodynamics and Lagrangian transport are compared for the years 2012–2019, with a focus on 2016. We evaluate hypotheses for *P. australis* introduction, effects of changing hydrodynamics on the 2016 bloom, influences of Scotian Shelf processes on the GOM in 2016, potential links to other *P. australis* populations in the North Atlantic, and implications of this research for future studies and monitoring practices.

2 Methods

2.1 Study Site – The Gulf of Maine

The GOM lies between Cape Cod, MA, USA at 42°N and the Bay of Fundy, Canada at 44.5°N (Figure 1A). Sea surface temperatures range from 6°C in the winter to 22.5°C in the summer, and salinity ranges from 29 PSU near the coast to 33.5 PSU offshore (Li and He, 2014). It is considered a gulf because its offshore boundaries, Georges Bank and Browns Bank, are shallower than 100m, while its three major basins – Georges Basin, Jordan Basin, and Wilkinson Basin – are deeper than 200m (Townsend et al., 2006). Gulf inflows occur via the Northeast Channel and south of Nova Scotia. The general circulation around the GOM is cyclonic, and outflows occur via the Great South Channel and the Northeast Channel (Brooks, 1985; Lynch et al., 1997; Pettigrew et al., 2005; Xue et al., 2000). Water properties in the GOM interior are set by the water mass properties at the inflow locations: Northeast Channel deep inflows are a mix of relatively warm and salty Warm Slope Water and slightly cooler and fresher Labrador Slope Water, while Nova Scotia surface inflows are made up of cool, fresh Scotian Shelf Water (Smith et al., 2012; Townsend et al., 2015).

Field Data 81 2.2 82 The Department of Fisheries and Oceans Canada (DFO) has conducted annual summer surveys 83 of the Scotian Shelf since 1970. In 2016, the survey was conducted from June 28 to Aug 15, and 84 a total of 250 stations were sampled with Conductivity-Temperature-Depth (CTD) profiles (Figure 85 1b). At the surface, 50m, 100m, and the bottom, temperature and salinity values were 86 interpolated onto a 0.2-by-0.2 degree grid via optimal interpolation (Hebert et al., 2018). 87 NERACOOS buoys have recorded temperature, salinity, conductivity, potential temperature, air 88 temperature, air pressure, and wind speed at hourly intervals since 2001 (Morrison, 2019) (Figure 89 1). Instruments were positioned at 1, 20, and 50+ m below the surface (site-depending), allowing 90 for characterization of the vertical structure of the water column at high temporal resolution. 91 Salinity and temperature data from buoys N, M, and I from 2001–2019 were used to characterize 92 water mass characteristics and climatology. 93 94 95 96 97 98

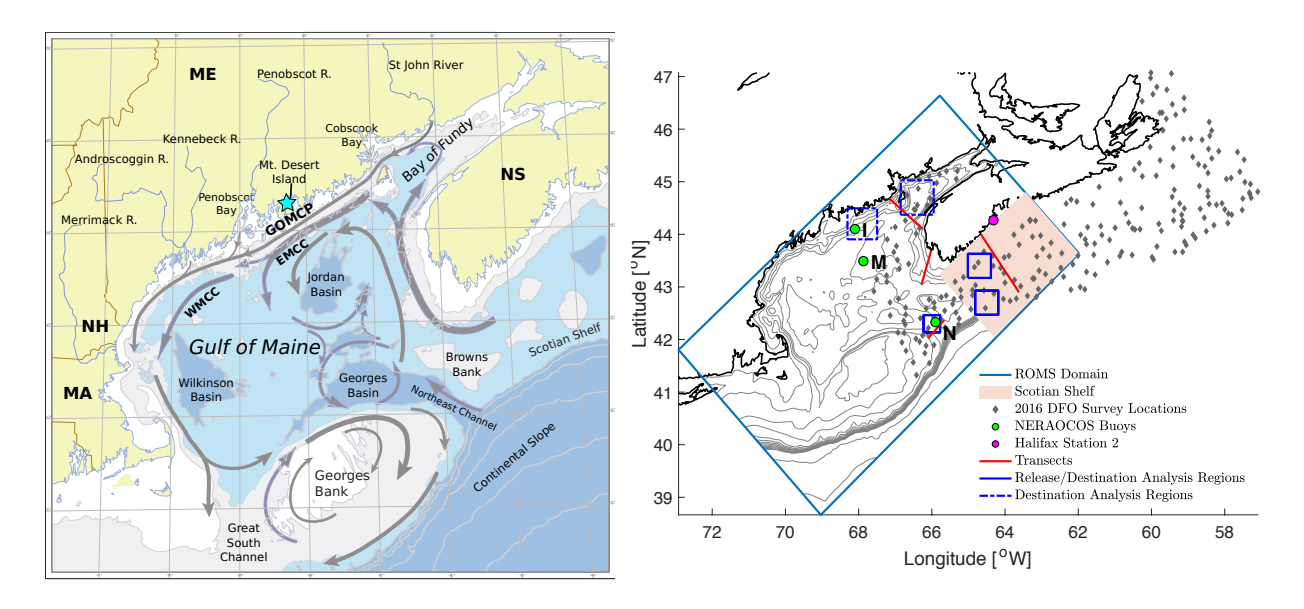


Figure 1 – (left) Climatological circulation of the GOM as described in Pettigrew et al. (2005) and adapted in Anderson et al., (2005)⁴. GOMCP stands for Gulf of Maine Coastal Plume, WMCC stands for Western Maine Coastal Current, and EMCC stands for Eastern Maine Coastal Current. Two-letter abbreviations are for Massachusetts (MA), New Hampshire (NH), and Nova Scotia (NS). (right) Map of the Gulf of Maine showing the ROMS domain (blue box), the Scotian Shelf portion of the ROMS domain (red shaded box), NERACOOS buoys (green circles), Halifax Station 2 (magenta circle), 2016 DFO survey locations (grey diamonds), transects for analysis (red lines), and particle analysis regions (solid blue boxes are sources and destinations, while dashed blue boxes are destinations only). The contour lines are drawn at 25m, 50m, 75m, every 100m to 1000m, and 2000m.

2.3 Models

2.3.1 Hydrodynamic Model

The Regional Ocean Modeling System (ROMS) is a free-surface, hydrostatic, primitive equation circulation model with split-explicit time-stepping for the baroclinic and barotropic modes (Shchepetkin and McWilliams, 2005). It has been applied to the GOM, where it is used annually to forecast *A. catenella* blooms (He et al., 2008). The GOM ROMS configuration includes 36 terrain-following sigma layers, 1-km resolution inshore, and 3-km resolution offshore. The model domain stretches from Georges Bank and Cape Cod in the Southwest to the Bay of Fundy and Halifax in the Northeast (Figure 1), encompassing 38 to 47°N and 61 to 73°W. Other models have been developed for the region, including an operational model for the Gulf of Maine using the

⁴ The left panel was published in Deep-Sea Research II, Vol 52, Anderson, Donald M., Keafer, Bruce A., McGillicuddy, Dennis J., Mickelson, Michael J., Keay, Kenneth E., Libby, P. Scott, Manning, James P., Mayo, Charles A., Whittaker, David K., Hickey, J. Michael, He, Ruoying, Lynch, Daniel R., Smith, Keston W. "Initial observations of the 2005 *Alexandrium fundyense* bloom in southern New England: General patterns and mechanisms." p. 2858, Copyright Elsevier (2005)

Finite Volume Coastal Ocean Model (FVCOM) (Beardsley et al., 2013; Chen et al., 2013), which has an unstructured grid that can allow for finer resolution of complex coastal geometry. ROMS was chosen for this study, however, because it is part of an existing framework that benefits from extensive model development and assessment in previous circulation and HAB studies in the region (e.g. He et al., 2008; Li et al., 2020, 2015, 2009; McGillicuddy et al., 2014, 2011). In addition, this study focuses on the large-scale low-frequency hydrodynamic variability, for which ROMS and FVCOM solutions are very similar. The choice to use ROMS also lays the foundation to develop future Pseudo-nitzschia models in the same manner as the existing A. catenella model. Three-dimensional temperature, salinity, and velocity, and two-dimensional sea surface height from HYCOM (HYbrid Coordinate Ocean Model) (Wallcraft et al., 2003) were interpolated to the ROMS grid to create initial and boundary condition files. HYCOM experiment GOFS3.0, with 33 vertical layers and 1/12° horizontal resolution, was used for years 2012–2018, while GOFS3.1, with 41 vertical layers and 1/12° horizontal resolution, was used for year 2019, because GOFS3.0 was only available through November 2018. HYCOM utilizes hybrid vertical coordinates, with isopycnal vertical layers in the open stratified ocean, terrain-following sigma layers in the coastal ocean, and z-coordinates in unstratified areas. HYCOM also assimilates data from the Navy Coupled Ocean Data Assimilation (Cummings, 2005) and estimates surface fluxes with bulk parameterization and data from the Navy Operational Global Atmospheric Prediction System (NOGAPS). Atmospheric forcing in the GOM ROMS was parameterized via bulk formulation with data from the North American Regional Reanalysis (NARR) (Mesinger et al., 2006), which assimilates data from various sources to calculate air temperature, air pressure, wind speed, cloud fraction, longand shortwave radiation, relative humidity, and precipitation. Output resolution was 6 hours and 1/6°. Five rivers are included in the GOM ROMS forcing files as volumetric transport (m³ s⁻¹) as measured by the U.S. Geological Survey (Interior, 2021): (in order of decreasing transport) St. John River, Penobscot River, Kennebeck River, Androscoggin River, and Merrimack River. A volumetric adjustment was added during forcing file generation to account for drainage area downstream of the gauge.

117

118

119

120

121

122

123

124

125

126

127

128

129

130

131

132

133

134

135

136

137

138

139

140

141

142

143

For each year from 2012 to 2019, GOM ROMS was initialized in February and run through December. These years were chosen to compare four non-*P. australis* years (2012–2015) with the four years after *P. australis*' first appearance (2016–2019). Each year was initialized with HYCOM output to reduce potential error caused by model drift over time. Because of strong tidal variability in the region, model results were saved hourly for use with the particle tracking model.

2.3.2 Particle Tracking Model

The Lagrangian TRANSport Model (LTRANS) is an offline, three-dimensional particle tracking model (Hunter 2020; North et al., 2008, 2006; Schlag and North, 2012). It reads in the output from ROMS and calculates particle trajectories through a combination of advection (4th Order Runge-Kutta advection scheme), turbulence, and particle behavior. Turbulence was parameterized with a random walk model in the horizontal and a random displacement model in the vertical, with horizontal diffusivity set to 2 m² s⁻¹ and vertical diffusivity taken directly from ROMS. Particles in these simulations were passive and neutrally buoyant. LTRANS operates on the native ROMS grid, using bilinear interpolation in the horizontal and spline interpolation in the vertical to interpolate velocities, temperature, and salinity to sub-grid scales. Land-ocean boundaries are reflective, as is the surface boundary, and open ocean boundaries allow particles to escape the domain, but not reenter. For all experiments listed below, the internal time step for particle movement was two minutes, the external time step (from GOM ROMS) was one hour, and particle tracking results were saved every 6 hours.

2.3.3 Particle Tracking Experiments

A series of reverse and forward particle tracking experiments were designed to explore three related questions: (1) what are the most likely source regions for *P. australis*, (2) which of the source regions had the strongest connectivity to locations where contaminated shellfish and *P. australis* were observed, and (3) was the connectivity from source regions to the GOM different in 2016 compared to previous and subsequent years?

LTRANS was run "in reverse" by multiplying the velocities by -1 and reversing model fields (salinity, temperature, and velocity) with respect to time. The accuracy of this method was checked by plotting individual particle tracks without turbulence in the reverse and forward runs

and ensuring that they matched. Particles were seeded at each of the 2016 ship survey sample locations in Clark et al., (2019) at 1m, 10m, and 20m, in accordance with sample depths. 2,000 particles total were released at each unique (x,y,z) location, according to the method outlined in Simons et al. (2013). The particles were distributed evenly with one release at each location every 6 hours during the period of shipboard observations (Oct 5 00:00 to Oct 7 18:00) for a total of 420,000 particles. In addition to focusing on the timing of the 2016 ship survey, this release time period was sufficient for capturing the stochasticity of reverse connectivity, as the particle tracks fully sampled the known inflow pathways in the region (Section 3.2.1). The experiment was repeated in each year from 2012 to 2019 and run backward to the beginning of June (120 days). The forward experiments were designed to complement, and were guided by, the reverse experiments. A preliminary analysis of the reverse experiment pointed to the inner Scotian Shelf and Northeast Channel as the two most likely source regions for P. australis. For each forward experiment, a latitude-longitude point was made the center of a square with side lengths that were chosen to encompass the region of interest (see Table 1). Particles were randomly distributed horizontally within the square at a density of 3 particles km⁻², which was informed by the methods in Simons et al. (2013). At each (x,y) point, particles were released at the bottom, at mid-depth, and at 50m, 25m, and 1m. Particles were released every six hours for 3 days starting at midnight on July 15, August 1, and September 1 of each year and experiments were run through October 5. A six-hour release interval was chosen to avoid aliasing the tidal signal, and the three months were chosen to include mesoscale and other low-frequency variability. At the Northeast Channel (NEC) 9,375 particles were released at one time, and on the inner Scotian Shelf (SS) 15,360 particles were released at one time. This totals 121,875 (NEC) or 199,680 (SS) particles per location-release, 365,625 (NEC) and 599,040 (SS) particles per location (July, August, and September combined), 964,665 particles per year (2 locations and 3 release times), and 7,717,320 particles in all.

198

173

174

175

176

177

178

179

180

181

182

183

184

185

186

187

188

189

190

191

192

193

194

195

196

197

Table 1 - Locations of particle releases for the forward experiments.

Release Location	Center latitude/longitude	Region Side length (km)
Inner Scotian Shelf	43.4, -64.7	32
Northeast Channel	42.3, -66.0	25

201 2.4 Data Analysis

2.4.1 Field Data and ROMS

To see if the hydrographic conditions or transport pathways were distinct in 2016, both model output and observations were used to plot water mass properties, velocity, transport, and vertical water column structure. For all analyses, ROMS output was extracted from the nearest grid cell to the observation location, rather than interpolated.

On the Scotian Shelf, ROMS surface and bottom salinity and temperature were averaged over the region between 42.55°N and 44.64°N and 65.53°W and 62.01°W (Figure 1A). Stratification was defined as the difference in potential density between the bottom and the surface.

ROMS results were further analyzed as transects. Four transects were chosen to capture various upstream locations from the 2016 sample site, where "upstream" was determined by knowledge of the climatological circulation and the results from the reverse particle tracking simulations. The four transects were on the Scotian Shelf (64.66°W, 44.00°N to 63.62°W, 42.9°N), south of Nova Scotia (66.57°W, 42.62°N to 66.02°W to 43.69°N), across the Northeast Channel (66.11°W, 42.02°N to 65.66°W, 42.37°N), and across the mouth of the Bay of Fundy (67.16°W, 44.68°N to 66.26°W, 44.11°N) (Figure 1B). ROMS u and v velocities were projected in the alongshore direction according to the angle of the coast relative to East such that u > 0 was toward the GOM. In the Northeast Channel, velocities were projected parallel to the channel walls. Transport toward (away from) the GOM was calculated via

$$Transport = \sum_{i=1}^{N} u_i * A_i$$

where i is each grid cell where u > 0 (u < 0), u is the alongshore component of the velocity in grid cell i, A_i is the grid cell cross-sectional area, and N is the total number of grid cells where

223 u > 0 (u < 0).

224

Salt transport was calculated via

$$Salt Transport = \sum_{i=1}^{N} S_i * u_i * A_i$$

- where S_i is the salinity in grid cell i. Transport estimates were filtered with a weekly running
- mean before plotting to reduce the tidal signals.
- **228** 2.4.2 LTRANS
- 229 2.4.2.1 Particle Density and Particle Probability
- 230 To compare connectivity between one source region and multiple destination regions, particle
- 231 density was calculated by dividing the sum of all particles in the destination region by the region
- area (l^2 , where l is the side length defined in Table 1). This method was chosen to enable
- 233 comparisons between regions of different sizes. The destinations for the reverse run, the inner
- 234 Scotian Shelf (43.4°N, 64.7°W, l = 32km) and Northeast Channel (42.3°N, 66.0°W, l = 25km),
- were the same as the forward release locations (Table 1).
- 236 For intra- and interannual comparisons in connectivity, particle probability was calculated
- 237 according to

241

242

243

244

238
$$probability = \frac{\sum particles \ within \ region}{P_i} \times 100\%$$

where P_i is the total number of particles initially released from the source region. The destination

regions were the Bay of Fundy, centered on 44.7°N, 66.4°W, with a side length of 50km, and the

eastern Maine coast, centered on 44.2°N, 67.9°W, with a side length of 45km (Figure 1B). The

Bay of Fundy was chosen because it was where the 2016 bloom was first observed. The location

along the eastern Maine coast was based on the 2016 ship survey location in Clark et al. (2019)

and subsequent reports of shellfishery closures in eastern Maine.

2.4.2.2 Growth Delivery Potential

245

246

247

248

249

250

251

252

253

254

255

256

257

258

259

260

261

262

263

264

265

266

267

268

269

270

271

272

An estimate of potential growth for P. australis as a function of temperature was calculated for those particles that were in the Bay of Fundy at any point between September 5 and September 19, the two weeks leading up to when shellfish toxicity exceeded the regulatory limit (Canadian Food Inspection Agency, 2016). Growth rates were also estimated for particles in the Bay of Fundy between September 12 and 19, and results were similar to the two-week time period, so only the two-week time period is reported here. Temperature-based laboratory growth rates were measured for a Gulf of Maine P. australis isolate obtained from the 2016 toxic bloom. The isolate was maintained in batch culture in sterile GOM seawater (salinity 33 PSU) amended with f/4 nutrients at 13°C under a 12:12-hour light:dark cycle with cool-white light at ~150 µmol photons m⁻² s⁻¹. For acclimatized growth rates, cells were transferred to a thermal-gradient device (Blankley and Lewin, 1976) while keeping other growth conditions the same. Growth was monitored by measuring in vivo fluorescence daily with a Turner AU-10 Fluorometer (Turner Designs, San Jose, CA). After reaching steady state growth (i.e., for 3 generations) at 13°C, the culture was similarly acclimatized to additional temperatures (7, 9, 11, 13, and 15°C) using a stepwise increase or decrease of 2°C. If positive growth was achieved for a given temperature, the culture was transferred to a new temperature after three generations, even if not in steady state. To calculate per-particle potential daily growth, each particle's along-track temperature was extracted on days when it was entirely in the euphotic zone (defined as 100m according to the data on NASA's Ocean Color Website, Feldman, 2014) and averaged over the entire day. Euphotic zone depths of 50 and 75m were also tested with no discernible changes to the results. Growth rate at each daily temperature was assigned via linear interpolation of the growth curve. On days when the particle exited the euphotic zone, the growth rate was set to zero. Per-particle average potential daily growth rate was calculated over each particle's trajectory by dividing the sum of daily potential growth rates by the number of days in the experiment. Interannual comparisons of the distributions of average potential daily growth rate were done

with the Kolmogorov-Smirnov test. This pair-wise test compares the maximum difference

between two empirical distributions to a theoretical maximum difference to determine the likelihood that the two samples are from the same distribution. It does not assume normal distribution.

2.5 Model Validation

ROMS has been used for many years to study circulation and *A. catenella* (formerly *A. fundyense*) blooms in the GOM (Fennel and Wilkin, 2009; He et al., 2008; Li et al., 2015, 2009; López et al., 2020; McGillicuddy et al., 2011). From a comparison between ROMS data and coastal CTD casts and NERACOOS moorings, Li et al. (2009) found that the model accurately captured surface and sub-surface temperature, salinity, and velocity to reproduce the general hydrodynamics along the coast on monthly and seasonal time scales, but that it missed processes on an event-by-event basis and at local scales. Our analysis agrees with this assessment.

ROMS accurately depicted the GOM's climatic circulation, with cyclonic circulation in the gulf interior, anticyclonic circulation around Georges Bank, inflows via Nova Scotia and the Northeast Channel, and outflows via the Northeast Channel and Great South Channel (Figure 2, compare with Figure 1A). The model also depicted the episodic nature of Northeast Channel inflows: at depth (>100m) near NERACOOS buoy N, both ROMS and the observations showed changes in salinity up to 2 PSU and changes in temperature up to 6°C in as little as a week (Figure S-1 in the Supplementary Material). The model also captured seasonal and spatial patterns in sea surface temperature: time series of model output vs NERACOOS Buoy measurements and Halifax Station 2 were in good agreement (Li *et al.*, 2009). On the Scotian Shelf, ROMS estimates of water mass properties were in general agreement with observations from the 2016 DFO Surwey on the Scotian Shelf were -0.22°C (Surface), 0.47°C (50m), -1.42°C (100m), and -1.10°C (Bottom). The mean salinity biases from the DFO Survey in the same time period were 0.30 PSU (Surface), 0.09

Although the mean biases in temperature and salinity over the Scotian Shelf were overall small, point comparisons between the observations and ROMS output revealed local inaccuracies in model predictions. This emphasizes the need to focus on long-term, low-frequency processes. At

PSU (50m), -0.32 PSU (100m), and -0.38 PSU (Bottom).

some locations, ROMS inaccurately simulated salinity: at Halifax Station 2, surface salinity in the model was more saline than observations by up to 1.8 PSU (Supplementary Material Figure S-3), while salinity at depth was fresher than the DFO observations by up to 0.3 PSU (Figure 4). The disagreement at depth could be partly due to the scarcity of nearshore observations in the survey, but inshore salinity values in ROMS were often fresher than observations. Despite these inaccuracies, ROMS represented the key spatial gradients in the salinity distribution: increasing salinity with depth and with distance from shore. At NERACOOS buoy I, 50m modeled salinity was sometimes fresher than observations by up to 1.3 PSU (Supplementary Material Figure S-4). Finally, ROMS did not capture the rapid increase in salinity (~0.5 PSU over 6 days) observed at 250m at NERACOOS Buoy M in July 2016 (Clark et al., 2019). However, as mentioned above, ROMS did have rapid changes in salinity at the Northeast Channel and episodic salinity inflows, which are the processes thought to drive the rapid salinity increase at Buoy M. ROMS captures key features that are relevant to the research questions in this study. Because the model captures the alongshore flow along the coast of Maine, bloom progression and P. australis connectivity in the gulf interior can be addressed. With the model's representation of Northeast Channel and Nova Scotia inflows, the P. australis gulf introduction hypothesis can be tested. Third, because the model captures both high salinity pulses at the Northeast Channel and the location and magnitude of the observed near-bottom salinity on the Scotian Shelf in 2016 (Figure 4), potential origins of the high salinity signal near the coast of Maine in 2016 (Clark, et al. 2019) can be explored. For the purposes of this paper, ROMS is used to draw relative comparisons between years and locations, because large-scale, low-frequency flow is accurate in spite of local disagreements. In addition, large-scale patterns in salinity allow for analysis of nearshore vs. offshore inflow routes and water mass changes with depth. The model is also used to assess interannual variations in connectivity, inflows through the Northeast Channel, and water mass properties on the Scotian Shelf, to compare 2016 to the other years from 2012 to 2019, and to evaluate P. australis

301

302

303

304

305

306

307

308

309

310

311

312

313

314

315

316

317

318

319

320

321

322

323

324

325

326

327

introduction hypotheses.

Yearly Averaged Circulation in the GOM in 2016 from ROMS

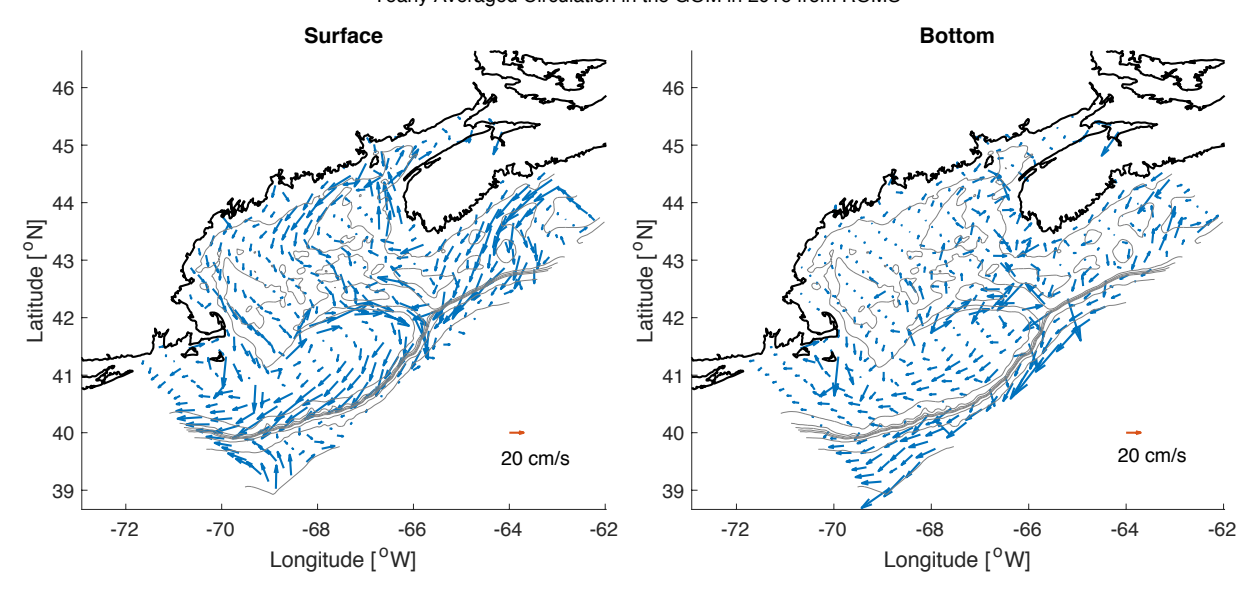


Figure 2 – Year-long averaged surface (left) and bottom (right) circulation in the Gulf of Maine in 2016 as simulated by ROMS. Output grid was decimated by a factor of ten before plotting. The scale of the velocity arrows is given in the bottom right.

ROMS-DFO Data Comparison in T-S Space

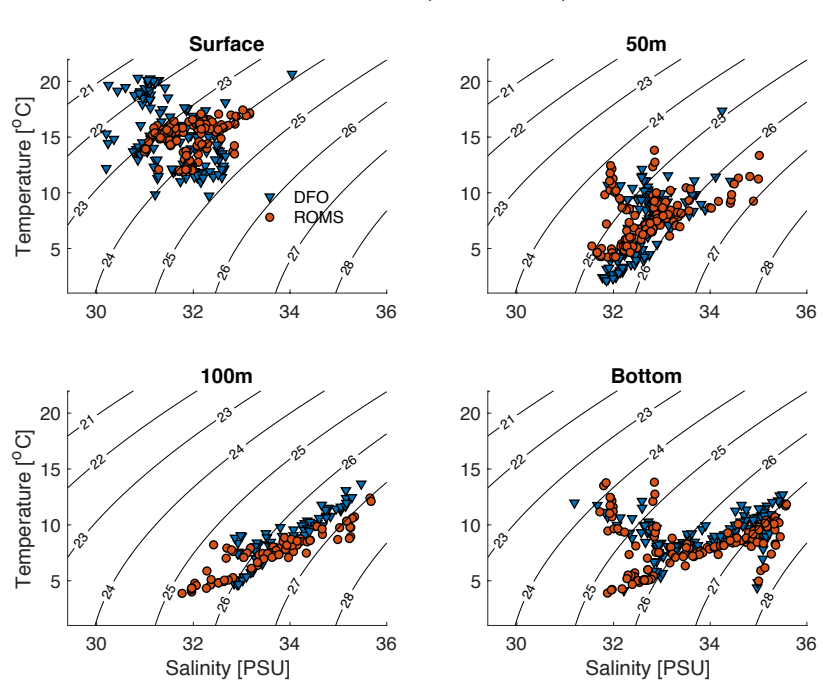


Figure 3 - ROMS (red circles) and DFO (blue triangles) temperature vs. salinity on the Scotian Shelf at (clockwise from top left) the surface, 50m, the bottom, and 100m. ROMS data were extracted from the nearest grid point to the DFO sample location.

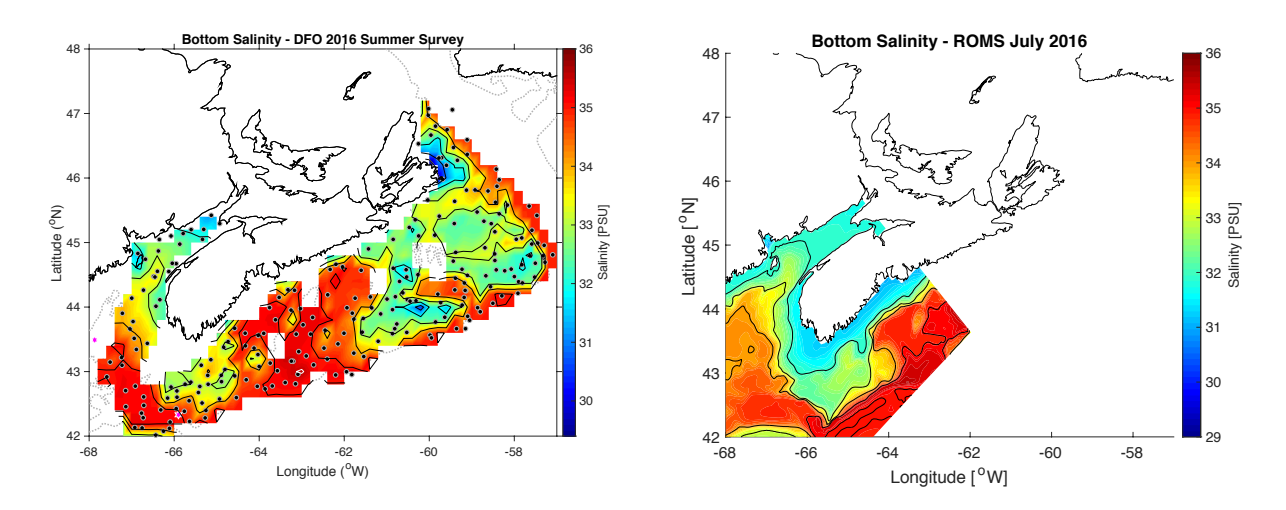


Figure 4—(left) Scotian Shelf bottom salinity as measured during the DFO Summer Survey in July, 2016. Black points indicate sample locations, and values are indicated by a color bar on the right. Spaces between sample locations were filled via optimal interpolation; (right) Bottom salinity as simulated by ROMS on July 15, 2016.

3 Results

3.1 Hydrodynamics from ROMS Output and Observations

3.1.1 Water Mass Properties

From the DFO survey in July 2016, bottom waters on the Scotian Shelf were anomalously warm (up to 4°C) and saline (up to 0.7 PSU) relative to the 1981–2010 climatology (Figure 5). Summer water mass properties are relevant to the fall bloom because of transport time scales (Section 3.2.1). Although ROMS did not capture the exact location of the anomalies, the model had relatively high salinity water (36 PSU) at a similar location to the observations (south of Halifax), as shown in Figure 4. Along with the increased salinity at depth, modeled sea surface salinity (SSS) decreased on the Scotian Shelf in 2016 compared to previous years (Figure 6): the annual average was lowest in 2017 and second-lowest in 2016 during the 8-year time period, with yearly minima in August 2016 and July 2017. Similarly, at Halifax Station 2, surface salinity (5–20m) in 2016 decreased below any other year in the 8-year time period besides 2013, and mid-depth salinity (50–100m) in 2016 and 2017 was less variable than in the other 6 years studied (Supplementary Material Figure S-8). However, given that the temporal resolution of the 2016 observations was

coarser than in the other years from 2012 to 2019, it is difficult to assess the significance of these changes.

3.1.2 Transport

At the same time and location that positive salinity anomalies were observed on the Scotian Shelf in July 2016, modeled volume and salt transport toward the GOM increased as a result of increased velocities and increased salinity (Supplementary Material Figure S-9). When the salt transport was calculated with just data from offshore (>80km from the coast), the results were qualitatively similar to the full transect. This occurred simultaneously with the decreased sea surface salinity (Figure 6), so the overall increase in salinity transport suggests that the offshore, deep salinity anomalies (Figure 5) dominated the transport signal. (The potential relationship between increased salinity transport yet decreased nearshore salinity in July 2016 is discussed more in Section 4.3.) In addition, transport was calculated at additional transects downstream of the Scotian Shelf transect (not pictured in Figure 1), and increased velocity and salt transport were consistent features along the shelf in mid-July 2016. This suggests an anomaly that propagated along the outer shelf.

3.2 LTRANS

The next section focuses on connectivity and potential growth estimates from the particle tracking experiments, with an emphasis on the August release. August was chosen as an illustrative release date, because the connectivity time scale from the October 2016 sample region to the inner Scotian Shelf and Northeast Channel in the reverse simulation was 30–60 days (see below), or early August.

3.2.1 Connectivity

The 2016 LTRANS reverse simulation indicates connectivity from the 2016 sample region to the Northeast Channel and the inner Scotian Shelf (Figure 7). Connectivity was quickest to the Northeast Channel, rising at about 20 days post release in early/mid-September, while connectivity to the inner Scotian Shelf increased about 30 days post release, or late August/early September (Figure 7). Coastal connectivity to the inner Scotian Shelf was roughly consistent once established. Meanwhile, connectivity to the Northeast Channel was more episodic, with peaks

near 20, 30, 45, and 65 days, possibly due to the highly variable nature of Northeast Channel inflows. Reverse connectivity to the Northeast Channel was greater than to the inner Scotian Shelf via the coast, but the majority of particles that initially passed through the Northeast Channel ultimately continued upstream onto the outer Scotian Shelf (Figure 7). Therefore, regardless of inflow pathway, the most likely source region for P. australis was the Scotian Shelf. The forward simulations complement the reverse simulations by illustrating connectivity between each source region and the Bay of Fundy, where toxicity was first observed in 2016, and the eastern Maine coast, where P. australis was observed in water samples (Bates et al., 2018; Clark et al., 2019). Regardless of release time, particles were more likely to pass through the Bay of Fundy if released from the inner Scotian Shelf than the Northeast Channel. In 2016 this difference in connectivity was up to an order of magnitude (Figure 8), and for all 8 years it ranged from a factor of 2 to a factor of 8 (Figure 9). In contrast, the likelihood of reaching the eastern Maine coast was within the same envelope of variability for particles released on the inner Scotian Shelf and in the Northeast Channel in all years (Figure 8, Figure 9). On average, about 70% of the particles released on the inner Scotian Shelf that passed through the Bay of Fundy also passed along the eastern Maine coast. Connectivity varied interannually (Figure 9), but from neither the inner Scotian Shelf nor the Northeast Channel did particles in 2016 have an increased probability of reaching either the Bay of Fundy or the eastern Maine coast relative to other years from 2012 to 2019. In addition, weekly variability in connectivity was as large as interannual variability: in a series of tests for 2016, connectivity differences between release dates August 1st, 7th, 14th, and 21st were as large as connectivity differences among the August 1st releases in all 8 years (not shown). Interannual differences are therefore considered insignificant in this context. Because of their proximity to the coast, particles released from the inner Scotian Shelf were associated with warmer and fresher water than particles released in the Northeast Channel (Figure 10). On average, the particles released in August on the inner Scotian Shelf that passed along the eastern Maine coast were 0.8°C warmer, 1.2 PSU fresher, and 7m shallower than those

released in the Northeast Channel that passed along the eastern Maine coast (Table 2). In 2016,

particles released on the inner Scotian Shelf that passed along the eastern Maine Coast were

382

383

384

385

386

387

388

389

390

391

392

393

394

395

396

397

398

399

400

401

402

403

404

405

406

407

408

409

typically 2°C warmer, 0.6 PSU fresher, and 14m shallower than particles released in the Northeast Channel that passed along the eastern Maine coast (Table 2).

Table 2 - Summary of average temperature, salinity, and depth (2016 mean and interannual mean) for particles released from either the inner Scotian Shelf or the Northeast Channel that passed through the 2016 ship survey region.

	Temperature Mean		Salinity Mean		Depth Mean	
Release	Overall	2016	Overall	2016	Overall	2016
Location						
Inner	11.3°C	11.5°C	32.1	31.8	33m	30m
Scotian Shelf						
Northeast	10.1°C	9.5°C	33.3	32.4	40m	44m
Channel						

3.2.2 Potential Growth

Growth rates were measured in laboratory experiments for 7, 9, 11, 13, and 15°C (Figure 11). As evidenced by high standard error, cells grown at 7 and 9°C did not achieve steady growth. Nevertheless, they maintained positive growth at both temperatures for multiple transfers and thus mean – rather than acclimated – growth rates were calculated. Growth rates were extrapolated beyond the 7–15°C range using the rate of change of growth with temperature (0.02 d⁻¹°C⁻¹ if T<12 and -0.03 d⁻¹°C⁻¹ if T>12). These rates were derived from the growth response of P. P0 australis maintained at 13°C following short-term exposure to temperatures <7°C and >15°C. To account for the variability across temperatures as well as the uncertainty associated with testing a single P1. P1 australis isolate, a growth curve was fit to the growth rates at 4, 7, 9, 11, 13, 15, and 18°C according to the function given in Thomas et al. (2012):

$$\mu(T) = ae^{bT} \left[1 - \left(\frac{T - z}{w/2} \right)^2 \right]$$

T is the temperature in degrees Celsius, w is the thermal niche width, and z is the location of the maximum of the quadratic portion of the function, or the temperature at which the growth curve

is tangent to the Eppley Curve (Eppley, 1972). Parameter a is the growth rate estimate at 0°C, and b is the Eppley coefficient, or the slope of the growth curve where growth rate rises as a function of temperature. Parameters a, b, z, and w were fit within defined bounds. The bounds for a and b were [0,1], which was informed by the values given in (Norberg, 2004). The bounds for z were [7,15] and the bounds for w were [10,20], which were based on the range of temperatures at which growth rates were measured. The best fit by nonlinear least-squares was achieved when a=0.198, b=0.0746, z=7, and w=15.75. These a and b values are the same order of magnitude as in Norberg (2004), and these z and w values are reasonable given the temperature values used in laboratory experiments. The sum of squared errors from this fit was 0.0026. The full growth curve is given in Figure 11 and the measured growth values are given with corresponding standard errors in the Supplementary Material, Table S-1. Because particles released from the inner Scotian Shelf were in warmer water, they had higher average potential growth rates than those released from the Northeast Channel (Figure 12). The largest potential growth rates generally occurred nearshore and in the Bay of Fundy, with occasional elevated growth rates farther offshore (not shown). The exception to this is the year 2012, the year of a marine heat wave (Pershing et al., 2015), when potential growth rates were

430

431

432

433

434

435

436

437

438

439

440

441

442

443

444

445

446

447

448

449

450

451

The Kolmogorov-Smirnov test indicated that potential growth rates from the inner Scotian Shelf were significantly higher than from the Northeast Channel, whether the growth rates were from all years combined or from 2016 individually. However, potential daily growth rates were neither significantly higher nor significantly lower in 2016 compared to other years from 2012 to 2019, regardless of release location.

higher at all locations and there was no cross-shore gradient (not shown).

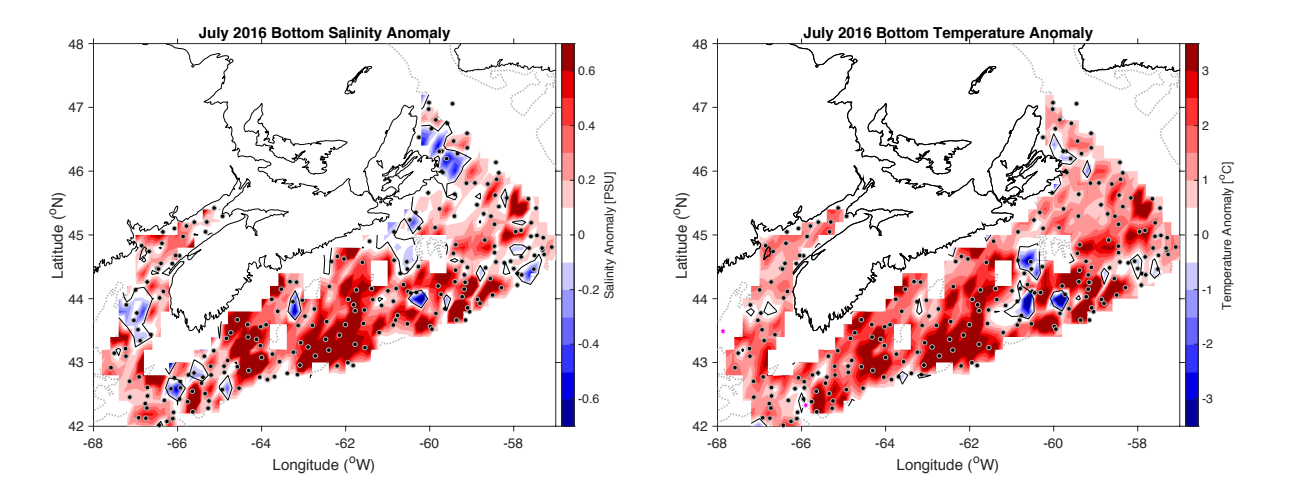


Figure 5 - Anomalies relative to the 1981–2010 climatology for (left) salinity and (right) temperature on the bottom of the Scotian Shelf in July 2016 as measured by the annual DFO Summer Survey.

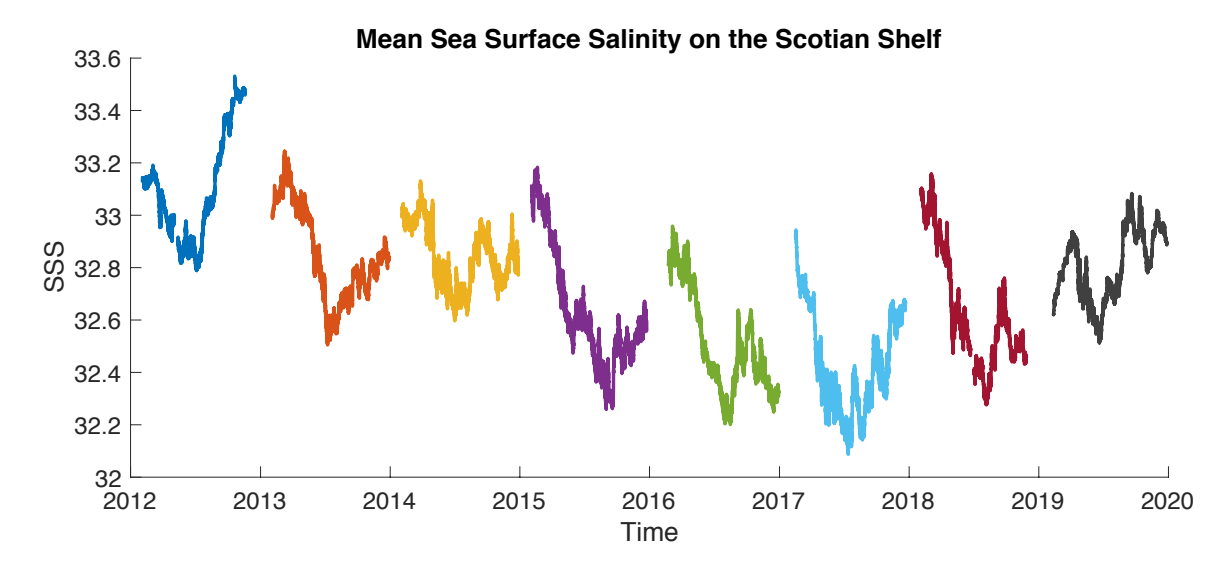


Figure 6 - Mean sea surface salinity (SSS) on the Scotian Shelf (as simulated by ROMS) vs time, from 2012–2019.

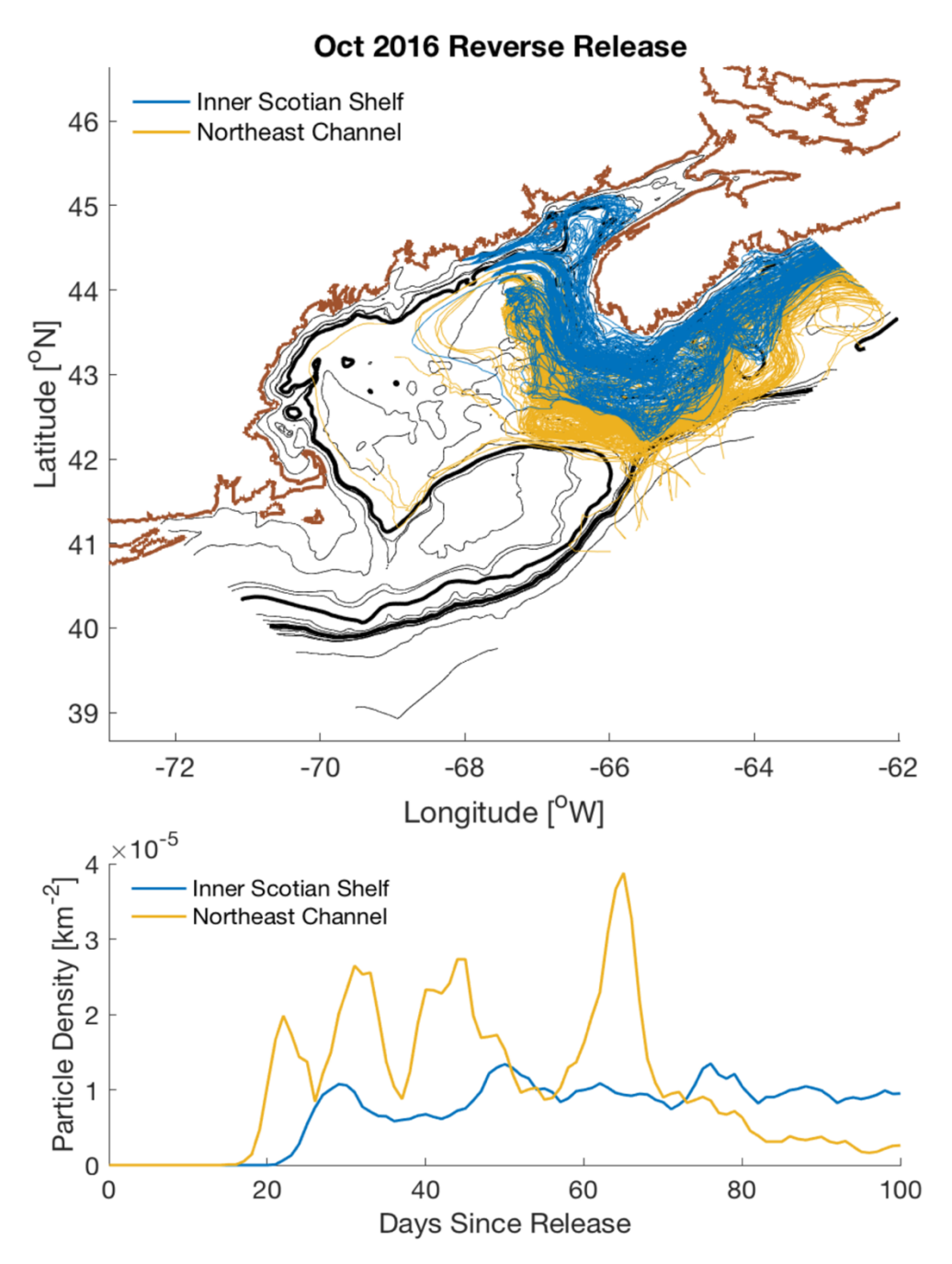


Figure 7 – (top) Particle tracks from the 2016 reverse simulation on a planar map of the Gulf of Maine. Tracks are color-coded by the first origin region the particle passes through: (blue) inner Scotian Shelf or (yellow) Northeast Channel. The thick brown contour indicates the shoreline, the thick black contours indicate 100m and 500m, and the thin black contours indicate 25m, 50m, 75m, every 100m to 1000m, 2000m, and 3000m. (bottom) Particle density for each of the potential transit regions (blue =inner Scotian Shelf; yellow = Northeast Channel) vs day since release from the 2016 reverse simulation. Particle densities are shown, rather than probabilities, because the Northeast Channel area is smaller than the inner Scotian Shelf.

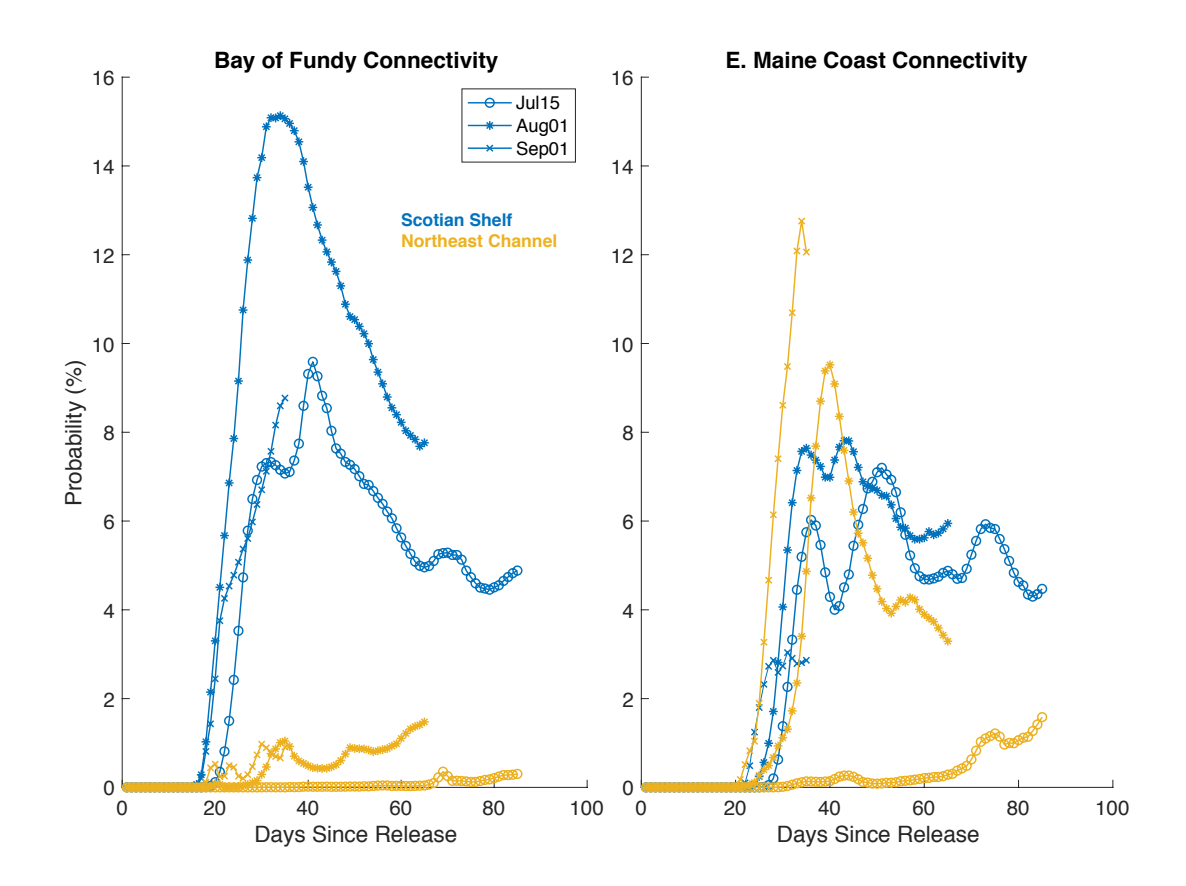


Figure 8 - Probability of a particle being in the Bay of Fundy (left) or E. Maine (right) vs. days since release as a function of release location (blue = inner Scotian Shelf; yellow = Northeast Channel) and release time in 2016 (o = July 15; * = August 01; x = September 01).

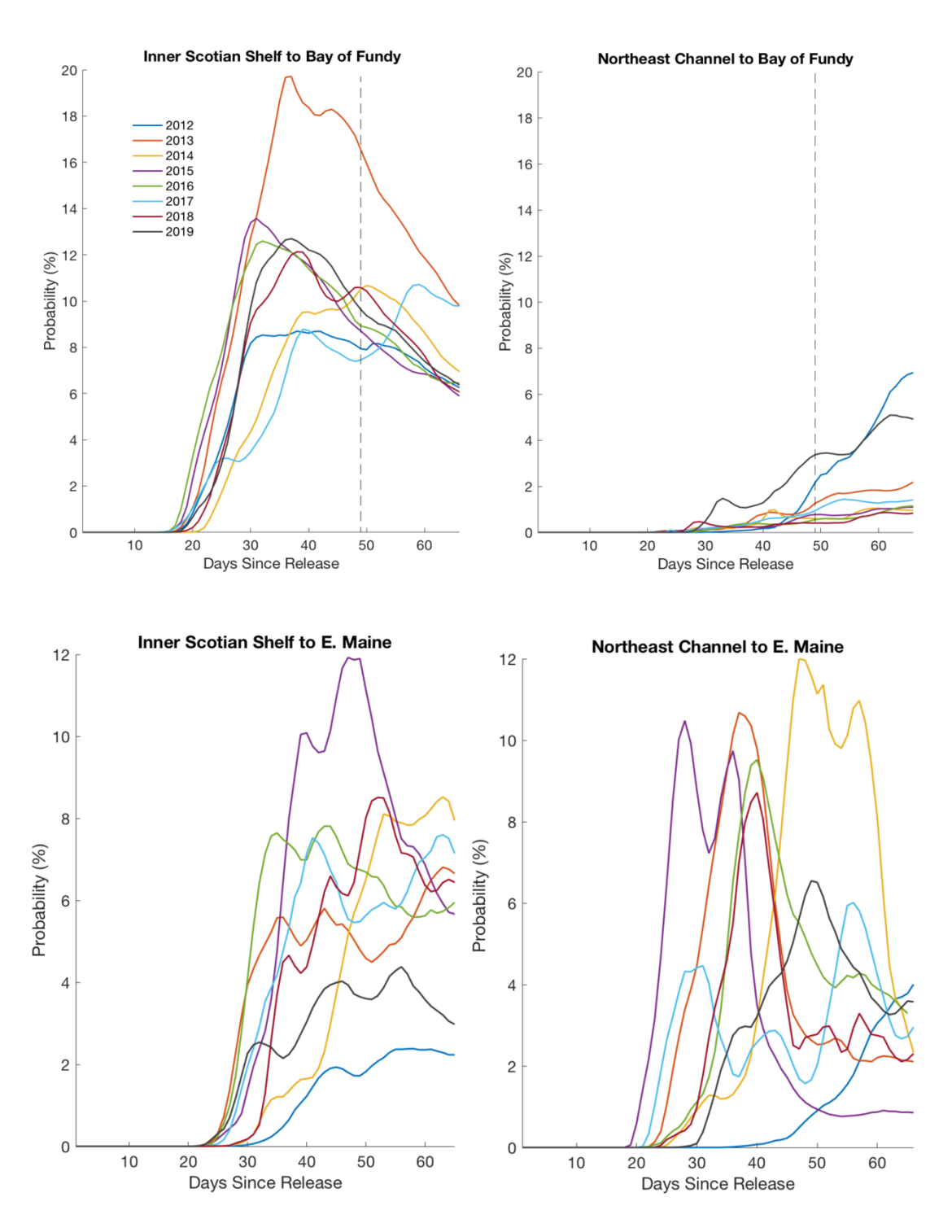


Figure 9 – Probability of being in the (top) Bay of Fundy or (bottom) E. Maine coast vs. days since release for particles released on August 1 on the inner Scotian Shelf (left) and in the Northeast Channel (right). Each year is represented by a different color, which is the same in all four plots. The vertical dashed line in the top plots indicates September 19, the time when toxic shellfish were first observed in the Bay of Fundy.

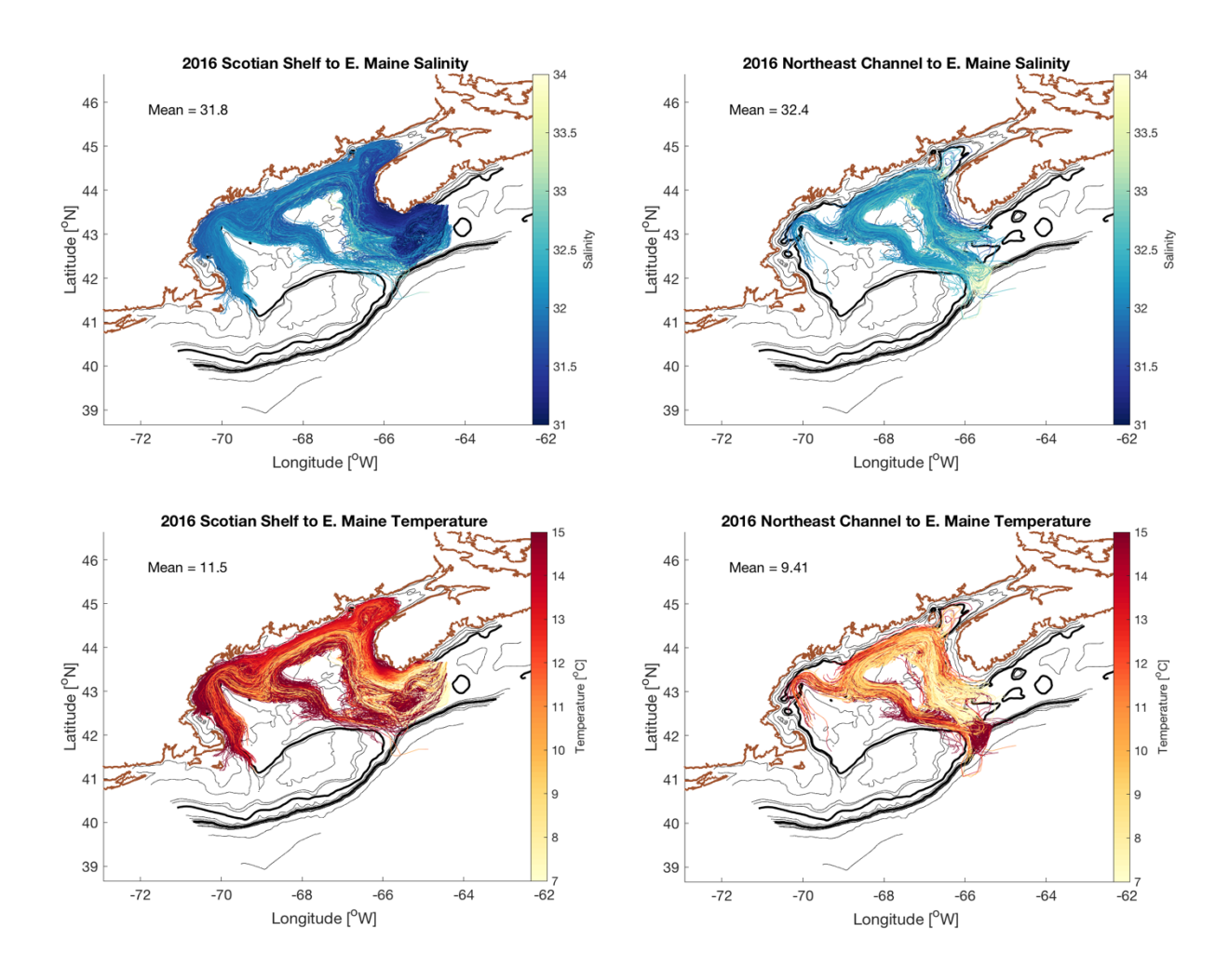


Figure 10 - Planar view of particle tracks in 2016 for particles released on August 1 from (left) the Scotian Shelf and (right) the Northeast Channel. Particle tracks are color-coded by (top) Salinity, or (bottom) Temperature, and colors are defined by the color bars on the right.

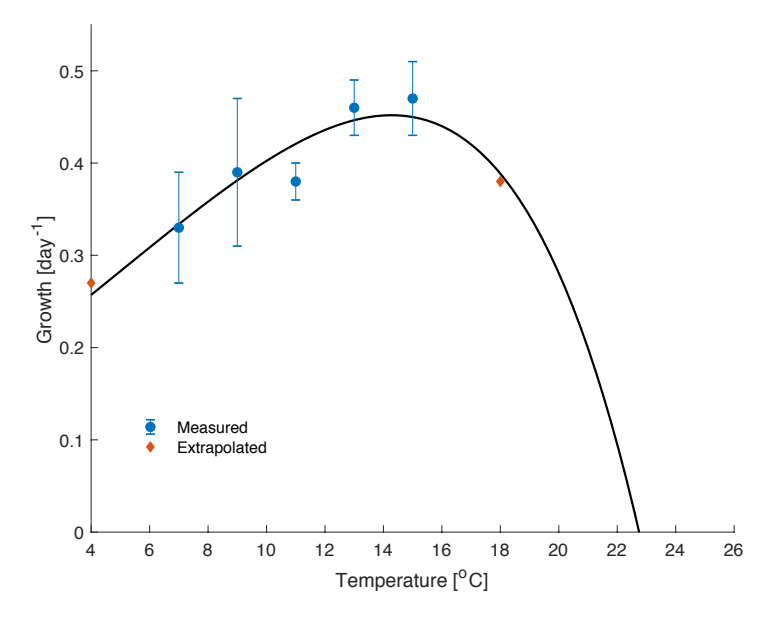
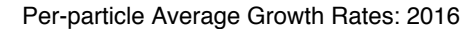


Figure 11 – Laboratory-based growth rates as a function of temperature as measured for a GOM P. australis isolate. The blue points indicate values that were measured, and the error bars show standard error. The orange diamonds were estimated using a rate of change of growth rate with temperature as measured during short-term exposure experiments. The black line shows the theoretical curve as estimated from the function given in Thomas et al. (2012).



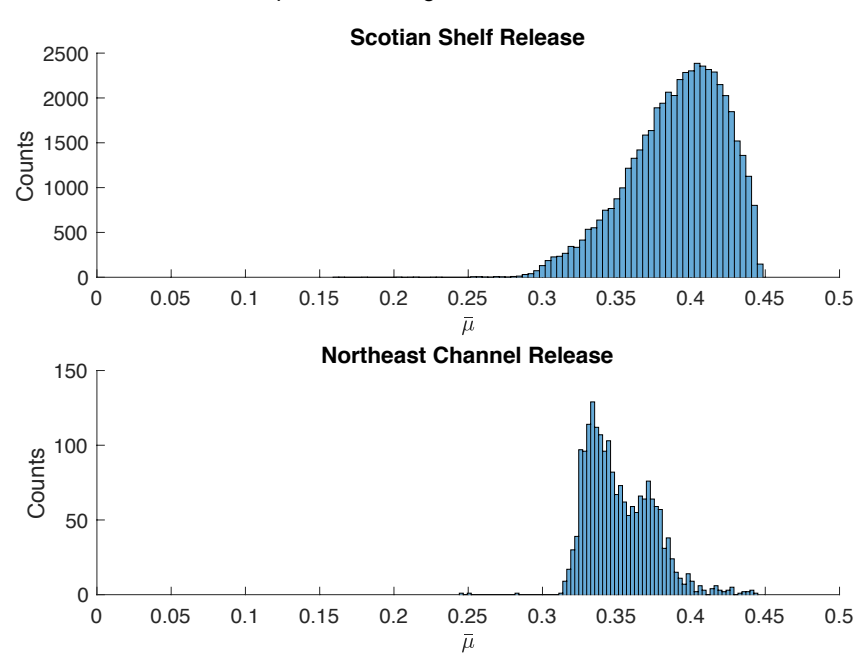


Figure 12 – Histograms of particle-averaged potential growth rates in 2016 for particles released on the inner Scotian Shelf (top) and in the Northeast Channel (bottom) that were in the Bay of Fundy between September 5 and September 19, 2016. Note that the y-axis scales are different.

4 Discussion

487

488

489

490

491

492

493

494

495

496

497

498

499

500

501

502

503

504

505

506

507

508

509

510

511

512

513

514

The particle tracking model, physical model, and *in situ* data provide clues regarding *P. australis* inflow route and timing, as well as changes to physical processes driving the 2016 bloom. The following section uses connectivity results from LTRANS and physical parameters from ROMS to determine the most likely inflow route. It also explores changes upstream that could have caused the 2016 event and hypothesizes the risk of regional *P. australis* HABs in the future.

4.1 Likely *P. australis* Introduction Pathway

The LTRANS reverse results indicate a P. australis source region on the Scotian Shelf, and inflow routes via either the Northeast Channel or around the southern tip of Nova Scotia. The current along the latter inflow route is not well defined in the literature, having been referred to as both "an extension of the Nova Scotia Current" (Townsend et al., 2015) and the beginning of the Gulf of Maine Coastal Current (Pettigrew et al., 2005). This route will therefore be called the coastal route for simplicity. In 2016, particles released in the Northeast Channel were as likely to reach the eastern Maine coast as those released on the inner Scotian Shelf, the majority of which were transported along the coastal route (Figure 8). From this alone, both the Northeast Channel and the coastal route were equally likely inflow routes for P. australis cells in 2016. However, particles released from the Northeast Channel had a low probability of reaching the Bay of Fundy compared to those released from the inner Scotian Shelf (Figure 8). An additional reverse experiment was run with particles released just below the surface in the Bay of Fundy from September 12 to September 19, which was the period of shellfish closures in that region. It confirmed that particles in the Bay of Fundy were connected to the inner Scotian Shelf via the coastal route, but were not connected to the Northeast Channel (Supplementary Material Figure S-12).

In addition to connectivity, along-path temperature and salinity provide important context. Particles that entered the gulf via the Northeast Channel were generally in a higher salinity range (Figure 10) than those that entered via the coastal route, although the salinity average was not as high as the coastal observations in Clark et al. (2019). However, particles that entered via the coastal route were more likely to be between 7 and 15°C, the range in which the GOM strain of

P. australis can sustain growth, than particles that entered via the Northeast Channel. The highest potential growth values occurred near the coast and in the Bay of Fundy, where water is shallower and warmer. As a result, potential growth rates were higher for particles coming in via the coastal route than for those coming in via the Northeast Channel.

Thus, there are arguments for and against both inflow routes, and particles entering both via the coastal route and the Northeast Channel connected to the eastern Maine coast. Northeast Channel particles were in a salinity range closer to the 2016 observations, but they lacked connectivity to the Bay of Fundy and were in relatively cool water. Meanwhile, coastal route particles had the strongest connectivity to the Bay of Fundy and were in a temperature range that promoted growth, but were in relatively fresh water. Despite the fact that the modeled salinity did not agree with the 2016 coastal observations, the warmer temperatures and connectivity to the Bay of Fundy mean that inflows via the coastal route were more likely to introduce *P. australis* than inflows via the Northeast Channel. In order for the cells to have been introduced to the Bay of Fundy before the first observation of toxic shellfish in mid-September 2016, they would have had to come from the Scotian Shelf sometime in or before early August 2016 and entered the Gulf of Maine near the coast of Nova Scotia.

4.2 2016 in an Interannual Context

A distinct aspect of the 2016 *P. australis* bloom compared to previous *Pseudo-nitzschia* blooms of other species in the Gulf of Maine is that it occurred in late September to October, while other observed blooms associated with DA had occurred from July to early September (Clark *et al.*, 2019; Fernandes *et al.*, 2014). The September bloom could be related to a "marine heat wave" that took place in 2016 across the GOM and Scotian Shelf (Pershing et al., 2018). From ship observations in 2016 (Clark et al., 2019, Figure 10B), sea surface temperatures along the coast of Maine in early October 2016 were warmer than the 2001–2016 October mean as measured at NERACOOS Buoy I, and as many as half of the measurements were more than one standard deviation warmer than the 2001–2016 October mean. The average water temperature from the ship observations was 13.5°C, which is near the optimal temperature for the tested strain of *P. australis* (Section 3.2.2, Figure 11). Increased temperatures have also been associated with

increased DA production on the U.S. West Coast (Trainer et al., 2020). Temperature has also been found to contribute to regime shifts between species of *Pseudo-nitzschia* near Denmark (Lundholm et al., 2010), and between zooplankton communities along the United States East Coast (Morse et al., 2017), although the shifts occurred over decades, not years. Therefore, increased temperatures may have been important for both growth and DA production in the GOM in 2016. The 2016 marine heat wave might also have selected against other organisms, whether competitive or predatory, to allow *P. australis* a greater chance to survive and grow. Water temperature effects on inter-community competition and long-term trends in the GOM are speculative and warrant further research.

Warmer temperatures may have supported a later bloom and more particles with relatively high growth potential in 2016, but the connectivity and potential growth rates that year were not significantly different from the other years between 2012 and 2019. Although the warm temperatures could have provided favorable growth conditions at other locations within the Gulf of Maine, they did not correspond with improved growth delivery potential along the inflow routes. It should be noted that the growth model used here incorporated only temperature-dependent growth rates. Although growth rates as a function of salinity have been reported for other strains of *P. australis* (Ayache et al., 2020), they are not currently available for this strain. To improve our understanding of bloom dynamics in the region, it is important to explore the growth rate estimates as a function of salinity, irradiance, and nutrients, as these can vary considerably depending on when and where cells occur. Expanding the model, however, is beyond the scope of this study.

4.3 Changes Upstream

On the Scotian Shelf in 2016, two changes occurred simultaneously: an increase in bottom salinity and a decrease in surface salinity. The increased bottom salinity, and its connection to elevated nearshore salinity in 2016 as explained in Clark et al. (2019), led to the "initial introduction" of *P. australis* hypothesis that motivated this study. The following section will explore this hypothesis more carefully, evaluate each salinity change separately, and investigate how the salinity anomalies relate to both each other and the 2016 DA event.

4.3.1 Increased Bottom Salinity on the Scotian Shelf

571

572

573

574

575

576

577

578

579

580

581

582

583

584

585

586

587

588

589

590

591

592

593

594

595

596

597

598

599

A notable change on the Scotian Shelf in 2016 was the increased bottom salinity in the summer, which was captured both by ROMS and by the DFO summer survey. Brickman, et al. (2018) observed and modeled these anomalies from 1990 to 2015 and argued that they occur as a result of warm, saline Gulf Stream water cutting off cool, fresh Labrador Current water near the Grand Banks off the coast of Newfoundland, Canada. Positive anomalies increased in frequency from 2006 to 2015, leading to more positive temperature and salinity anomalies at depth on the Scotian Shelf, but this might be the result of interdecadal variability in the region, rather than an indicator of a long-term trend (Brickman, et al. 2018).

The timing of the increased salinity on the Scotian Shelf (Figure 4) and the connectivity from the

Northeast Channel to the eastern Maine coast support the hypothesis that a salinity anomaly entered via the Northeast Channel. Brickman et al. (2018) estimated that salinity anomalies on the Scotian Shelf propagate southwest at about 150 km month⁻¹. The distance from the Scotian Shelf transect (where the increased salt transport was observed) to the Northeast Channel is about 230km, which means that the observed pulse would have taken about 1.5 months (45 days) to travel from the transect to the Northeast Channel, arriving at the Northeast Channel in mid-to-late August. From the model output, salt transport toward the Gulf of Maine across the Northeast Channel in mid-August increased more than one standard deviation above the interannual mean (as it did on the Scotian Shelf) and remained elevated for about 5 days. This salt transport was not larger than all other years from 2012 to 2019, and some years besides 2016 had summer salt transports of similar magnitude, but 2016 was the only year with elevated summer transport on both the Scotian Shelf and the Northeast Channel. Meanwhile, connectivity between the coast and the Northeast Channel in the reverse experiment in 2016 had a peak near 45 days post-release, or mid-August. This suggests that a water mass that was present on the Scotian Shelf in July and entered via the Northeast Channel in August could have arrived at the coast of Maine by early October, in time to be observed during the 2016 ship survey (Clark et al., 2019).

This discussion has focused on the timing of a particular anomaly observed in mid-July 2016, but as described by Brickman, et al. (2018), multiple anomalies can form on the Scotian Shelf in a

summer. Perfect timing is therefore not necessary for this introduction route to be plausible. Transport time varies with depth as a function of velocity shear: transport time scales from the Northeast Channel to the eastern Maine coast were calculated as a function of particles' initial depth and found to range from 45 days (surface to 50m release) to 90 days (bottom release). From the DFO survey data, anomalous salinity signals were present from 50 to 125m. Considering the range of possible depths and associated transport time scales, an anomaly passing through the Northeast Channel any time between early June and mid-August 2016 could explain the elevated salinity values at the coast.

Brickman et al. also hypothesized that repeated salinity anomalies would, through an integrative effect, result in deeper on-shelf penetration via channels such as the Northeast Channel. Considering that 2016 followed several years of increased bottom salinity anomalies on the Scotian Shelf (Brickman et al., 2018), it is not unreasonable that an anomaly would have reached the coast of Maine in 2016, causing the high salinity values observed in Clark et al. (2019). Given these lines of evidence, the saline water mass that was observed on the coast of Maine in 2016 likely came from the Gulf Stream, propagated along the outer Scotian Shelf, and entered the GOM through the Northeast Channel.

4.3.2 Decreased Sea Surface Salinity on the Scotian Shelf

As the bottom salinity on the Scotian Shelf increased in 2016, the surface salinity decreased by up to 0.6 PSU. Although the increased bottom salinity and decreased surface salinity occurred simultaneously in summer 2016 (Figure 5, Figure 6), bottom salinity and surface salinity on the Scotian Shelf were not consistently correlated across the 8 years studied. For each year, linear regressions were calculated between surface nearshore salinity and bottom offshore salinity at the ROMS eastern boundary (on the Scotian Shelf), and R² values ranged from 0.01 to 0.67, with an average of 0.16. Therefore, the surface and bottom salinity anomalies do not appear to be caused by the same process.

The modeled decrease in sea surface salinity on the Scotian Shelf in 2016 and 2017 (Figure 6) might suggest increased outflow from the St. Lawrence River via the HYCOM boundary conditions, because upper layer salinity (30–50m) on the Scotian Shelf is influenced by St.

Lawrence River discharge (Dever, et al., 2016). However, St. Lawrence River discharge was at an 8-year minimum in the 12 months prior to summer 2016 (Interior, 2021), and it has been shown that the salinity signal from the St. Lawrence River decreases to +/- 0.1 PSU by the time it reaches the Halifax Line (Ohashi and Sheng, 2013). It is therefore unlikely that changes in the St. Lawrence River caused the sea surface salinity changes on the Scotian Shelf. Townsend, et al. (2015) argued that there had been an increase in the frequency of strong Scotian Shelf Water inflows via Nova Scotia in the early 2010s, and presented evidence of increasing freshwater fluxes from the Labrador Sea via the Labrador Current. It is possible that the surface freshening modeled on the Scotian Shelf in 2016 and 2017 is indicative of these episodic changes. This is in contrast to the findings of Brickman et al. (2018), which outlined how the Gulf Stream effectively cuts off the Labrador Current near the Grand Banks, but this difference could be because the processes Townsend et al. described occur at the surface, while those described by Brickman et al. occur at depth. Intermediate layer water on the Scotian Shelf (50-100m, also known as the Cold Intermediate Layer, or CIL) is composed of either the inshore branch of the Labrador Current or CIL water formed in the Gulf of St Lawrence, which is distinct from St. Lawrence River outflow (Dever et al., 2016). In the intermediate layer at Halifax Station 2, observed salinity and temperature were both lower and less variable in 2016 than in the 7 other years in this study, with a water mass signature that was a mixture of Labrador Slope Water, Cabot Strait-Cold Intermediate Layer water, and Cabot Strait Subsurface water, as described in Dever, et al. (2016) (Figure 13). This suggests that changes on the Scotian Shelf are driven by changes in the Labrador Current or Gulf of St. Lawrence, either of which could be a link to the upstream source of *P. australis*. More work is necessary - either via an expanded model domain or ship surveys - to determine the relative likelihood of each source. To summarize, P. australis likely entered the Gulf of Maine via the inner Scotian Shelf and coastal route around southern Nova Scotia, was concurrent with decreased sea surface salinity on the Scotian Shelf, and had an upstream source in either the Labrador Current or Gulf of St. Lawrence. In contrast, the observed positive salinity anomalies on the Maine Coast likely originated in the

Gulf Stream and entered the GOM via the Northeast Channel. Particle tracking experiments

628

629

630

631

632

633

634

635

636

637

638

639

640

641

642

643

644

645

646

647

648

649

650

651

652

653

654

655

suggest that these two phenomena met along the upper coast of Maine and were mixed through strong tidal mixing, which is not unreasonable according to the data. If the positive salinity anomaly at the bottom (mean = 35) and negative salinity anomaly at the surface (mean = 32.5) were to mix, the required mixing ratio to achieve the salinity observed in Clark et al. (2019) (mean = 33.25) would be 30/70 (bottom/surface). The mixed water could have then flowed southwest where it was observed during the 2016 ship survey. For a more thorough analysis of environmental salinity and its correlations with different Pseudo-nitzschia species in the GOM during this period, the reader is referred to Clark et al. (2019). It should be noted that several studies have found salinity to influence *Pseudo-nitzschia* growth (Ayache et al., 2020; Doucette et al., 2008; Thessen et al., 2005) and DA production (Ayache et al., 2018; Thessen and Stoecker, 2008). In each of these studies, Pseudo-nitzschia growth and DA production increased with salinity, suggesting that the elevated salinity in 2016 might have played a role in the DA event. However, the year-to-year salinity differences discussed in this paper (order 1 PSU) are much smaller than those examined in the literature (order 5-10 PSU), so salinity is not thought to be the leading causative factor of the 2016 P. australis bloom or the associated DA event. This is discussed in more detail in Clark et al. (2019). Changing upstream water masses could also have affected nutrient concentrations in the GOM, and, in turn, the 2016 bloom. The surface and mid-depth salinity changes suggest increasing influence from the Labrador Current, which typically has a silica-to-nitrate ratio greater than 1 (Townsend et al., 2010). The bottom salinity anomalies, meanwhile, are thought to have originated in the Gulf Stream, which has a silica-to-nitrogen ratio less than 1 (Townsend et al., 2010). It is reasonable from a nutrient perspective that P. australis were carried in with the surface Scotian Shelf inflows, in that an increased silica-to-nitrogen ratio could have supported a diatom population. In the 2016 ship survey, however, the silica-to-nitrogen ratio was significantly lower compared to two of the previous years' ship survey samples, and this decrease was thought to exacerbate DA production (Clark et al., 2019). The low silica-to-nitrate ratio in the 2016 observations could be the result of Gulf Stream water mixing with Scotian Shelf water at the mouth of the Bay of Fundy, as hypothesized above. Thus, the two-pronged introduction hypothesis (P. australis via the coastal route and a positive salinity anomaly via the Northeast

657

658

659

660

661

662

663

664

665

666

667

668

669

670

671

672

673

674

675

676

677

678

679

680

681

682

683

684

Channel), in combination with the nutrient characteristics of the source water masses, suggest that *P. australis* was advected into the Bay of Fundy and eastern Maine, where it met saltier waters with low silica, enhancing DA production.

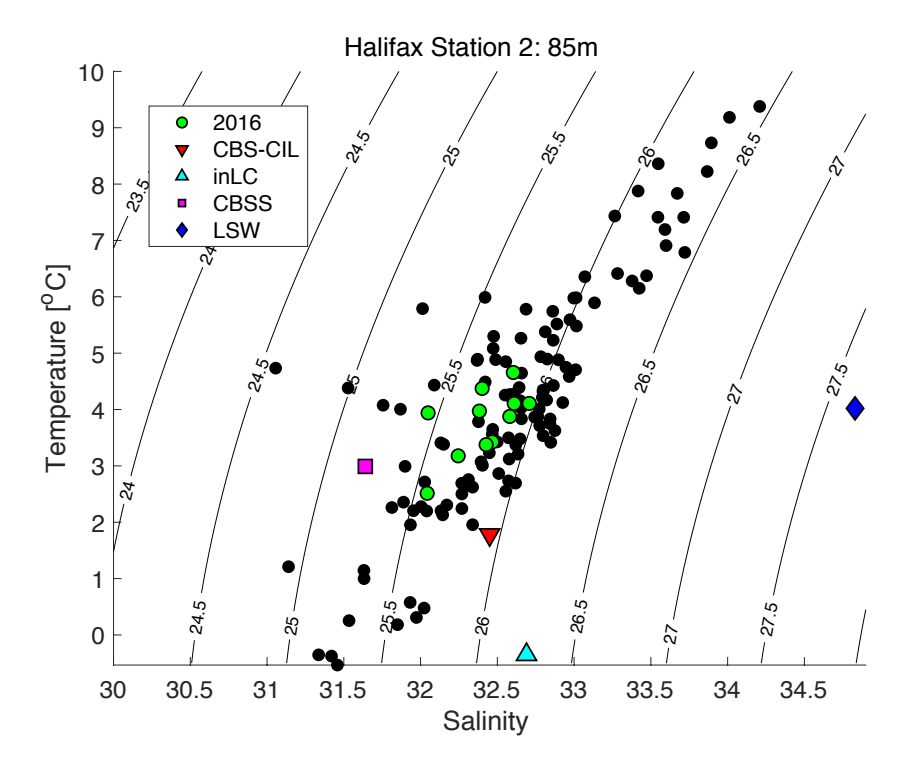


Figure 13 – Year-round temperature vs salinity as measured at Halifax Station 2 at 85m. 2016 is highlighted in green, while 2012–2018 are plotted in black. For comparison, the endmembers of CBS–CIL (Cabot Straight–Cold Intermediate Layer), in LC (Inshore Labrador Current), CBSS (Cabot Straight Subsurface Water), and LSW (Labrador Slope Water), as defined in Dever et al., (2016), are plotted.

4.3.3 *P. australis* Distribution in the North Atlantic

Evidence suggests that *P. australis* originated outside the GOM, which necessitates a look at *P. australis* distributions in the North Atlantic. *P. australis* has been observed near the United Kingdom and Ireland (Bresnan *et al.*, 2017, 2015; Cusack *et al.*, 2002; Fehling *et al.*, 2006; Hasle, 2002; Thorel *et al.*, 2014), France (Ayache *et al.*, 2020; Husson *et al.*, 2016; Klein *et al.*, 2010; Lema *et al.*, 2017; Thorel *et al.*, 2017), the Iberian Peninsula (Churro *et al.*, 2009; Palma *et al.*, 2010; Zapata *et al.*, 2011), and Morocco (Ennaffah *et al.*, 2012). The question remains how the cells could have been transported from these regions in the eastern Atlantic to the Scotian Shelf and Gulf of Maine.

The two likely transport routes are via the subtropical gyre and the Gulf Stream, or via the subpolar gyre and the Labrador Current, which meet near the Grand Banks of Newfoundland (Townsend et al., 2006). Introduction via the subtropical gyre would indicate a more southern origin of the species, possibly from Morocco or the Iberian Peninsula. To have been introduced along this route, the cells would have been carried west across the subtropical Atlantic and then northward by the Gulf Stream. However, growth rates of the 2016 GOM strain of P. australis declined rapidly at temperatures above 18°C (Figure 11), which is regularly exceeded along this route. In addition, we have argued that the source of *P. australis* was likely either the Labrador Current or Gulf of St. Lawrence. The strong connectivity from the inner Scotian Shelf to the Bay of Fundy and the decreased surface salinity on the Scotian Shelf in 2016 align with introduction via the subpolar gyre and Labrador Current. This suggests a cooler origin, which better aligns with the temperature growth curve for the GOM P. australis isolate. For comparison, P. australis from the English Channel grew best at 13.5–18.6°C, with growth rates from 0.47 to 0.83 day⁻¹ (Thorel et al., 2014). This temperature range overlaps with the range of peak growth for the GOM strain of P. australis, but it is slightly warmer and the growth rates are slightly higher. This could be due to population variability in the GOM that was not represented by examining a single GOM strain under the chosen laboratory conditions. Alternatively, selection may have occurred en route to the GOM. A subpolar introduction route seems more likely, but this hypothesis can be neither proven nor refuted without additional data. The best way to test this hypothesis is via targeted sampling, further culturing or modeling, and a genetic comparison between the GOM P. australis strain and other strains across the Atlantic, which could be the subject of future research.

4.4 Looking to the Future: Persistence vs. Persistent Introduction

703

704

705

706

707

708

709

710

711

712

713

714

715

716

717

718

719

720

721

722

723

724

725

726

727

728

729

730

An important question for scientists, managers, and state officials is whether the *P. australis* bloom in 2016 was anomalous or if it indicates a growing DA concern for the region. The 2016 event was likely due to the import of *P. australis* from the Scotian Shelf, but future blooms could be seeded by cells retained in the GOM, recurring introductions of cells from outside the GOM, or some combination of both. In other words, do we expect introduction plus persistence, or persistent introduction?

P. australis cells and DA-related shellfish harvest area closures have occurred in Maine every year since 2016 (Maine Department of Marine Resources, personal communication). *P. australis* cells are classified as a large-sized *Pseudo-nitzschia* species, and concentrations of large *Pseudo-nitzschia* cells at the Bar Harbor monitoring station exceeded 100,000 cells L⁻¹ in 2017, 2019, and 2020, with species-specific data being generated as part of an ongoing study. Low cell concentrations in 2018 could be the result of a spatially heterogeneous bloom in which cell concentrations were higher elsewhere, because data post-2016 are from a single-point time series.

However, despite observations of *P. australis* since 2016, the model output in this study did not point to any shifts that could explain why there were no DA events pre-2016 but annual DA events post-2016. Surface salinity was low in 2016 and 2017 and this corresponded with the original *P. australis* bloom in 2016 (Section 4.3.2), but the signal did not persist past 2017. In addition, model output did not indicate lasting changes in connectivity strength, connectivity timing, or growth potential. Evidence from the literature does point to long-term trends of increased inflows of Scotian Shelf Water (Townsend, et al. 2015) and increasingly warm/saline near-bottom water on the Scotian Shelf (Brickman, et al. 2018). This study did not identify any regime shift in water mass characteristics associated with the 2016 bloom, but other studies suggest changes in GOM inflows.

The evidence post-2016 indicates that *P. australis* blooms have continued in the GOM, but the available data are insufficient to determine whether the blooms are due to persistence or persistent introduction. Continued and expanded time series monitoring is recommended to map future blooms as they occur and to better understand interannual variability in the timing, extent, and severity of DA events in the region. Ideally this expanded effort would include sample collection on the Scotian Shelf and regions further upstream to better understand connectivity with established *P. australis* populations.

5 Conclusions

This paper used a physical model, particle tracking model, and observations to explore introduction and connectivity pathways to the Gulf of Maine in 2016, the year of a regionally

historic DA event. Results from the particle tracking simulations revealed that P. australis cells likely originated on the Scotian Shelf and were carried into the GOM via inflows south of Nova Scotia, because only this pathway explains the highly toxigenic P. australis cells and observed toxicity in the Bay of Fundy. Anomalously saline water originated near the bottom on the Scotian Shelf, entered the GOM via the Northeast Channel, and mixed with lower salinity surface water near the mouth of the Bay of Fundy. Regional connectivity and potential growth rates in 2016 were not larger than in the other modeled years between 2012 and 2019, but surface salinity on the Scotian Shelf was up to 0.6 PSU lower than the 7 other years in this study, and bottom salinity on the Scotian Shelf was 0.7 PSU greater than the 1981–2010 climatology. This suggests that the bloom was controlled by large-scale processes, not local-scale ones, and we propose that P. australis arrived at the Scotian Shelf and GOM via either the Gulf of St. Lawrence or the Labrador Current. Future studies should consider adding nutrient-, light-, or salinity-dependency to the growth model, exploring mechanisms underlying DA production in the GOM, expanding the hydrodynamic model domain to include offshore dynamics, and running the model continuously over more years to test the question of interannual persistence. Ocean sampling is recommended on and beyond the Scotian Shelf to determine if there is an upstream source of *P. australis*. Finally, P. australis blooms are likely to remain a concern in the GOM, and continued monitoring is warranted.

759

760

761

762

763

764

765

766

767

768

769

770

771

772

773

774

775

776

778 6 Acknowledgements

779 This research was funded by the National Science Foundation (Grant Number OCE-1840381), the 780 National Institute of Environmental Health Sciences (Grant Number 1P01ES028938), the Woods 781 Hole Center for Oceans and Human Health, and the Academic Programs Office of the Woods Hole 782 Oceanographic Institution. We thank Elias Hunter (Rutgers University) for his assistance with 783 LTRANS, and Yizhen Li (NOAA) for his assistance with ROMS. We thank Christina Chadwick and 784 Alexandra DeSmidt of the Florida Fish and Wildlife Conservation Commission for their assistance 785 with physiology experiments. We also thank the Department of Fisheries and Oceans Canada and 786 their Atlantic Zone Monitoring Program for sharing their field data. Data assimilative products 787 using HYCOM are funded by the U.S. Navy. Computer time was made available by the DoD High Performance Computing Modernization Program. The output is publicly available at 788 https://hycom.org. 789

- 791 CRediT author statement
- 792 **Suzanna Clark:** Conceptualization, Methodology, Software, Formal Analysis, Investigation,
- 793 Writing Original Draft, Visualization.
- 794 Katherine Hubbard: Conceptualization, Methodology, Resources, Writing Review & Editing,
- 795 Funding Acquisition.
- 796 **Dennis J. McGillicuddy, Jr.:** Conceptualization, Methodology, Resources, Writing Review &
- 797 Editing, Supervision, Funding Acquisition.
- 798 **David K. Ralston:** Conceptualization, Methodology, Resources, Writing Review & Editing,
- 799 Supervision, Funding Acquisition.
- 800 Sugandha Shankar: Methodology, Investigation, Writing Review & Editing

7 Bibliography

801

802 Anderson, D.M., Keafer, B.A., McGillicuddy, D.J., Mickelson, M.J., Keay, K.E., Scott Libby, P., 803 Manning, J.P., Mayo, C.A., Whittaker, D.K., Michael Hickey, J., He, R., Lynch, D.R., Smith, 804 K.W., 2005. Initial observations of the 2005 Alexandrium fundyense bloom in southern 805 New England: General patterns and mechanisms. Deep. Res. Part II Top. Stud. Oceanogr. 806 52, 2856–2876. https://doi.org/10.1016/j.dsr2.2005.09.004 807 Ayache, N., Herve, F., Lundholm, N., Amzil, Z., Caruana, A.M.N., 2020. Acclimation of the marine 808 diatom Pseudo-nitzschia australis to different salinity conditions: effects on growth, 809 photosynthetic activity, and domoic acid content. J. Phycol 56, 97–109. 810 https://doi.org/10.1111/jpy.12929 811 Ayache, N., Hervé, F., Martin-Jézéquel, V., Amzil, Z., Caruana, A.M.N., 2018. Influence of sudden 812 salinity variation on the physiology and domoic acid production by two strains of Pseudo-813 nitzschia australis. J. Phycol. 33, 0–3. https://doi.org/10.1111/jpy.12801 814 Bates, S.S., Hubbard, K.A., Lundholm, N., Montresor, M., Leaw, C.P., 2018. Pseudo-nitzschia, 815 Nitzschia, and domoic acid: New research since 2011. Harmful Algae 79, 3–43. 816 https://doi.org/10.1016/j.hal.2018.06.001 817 Beardsley, R.C., Chen, C., Xu, Q., 2013. Coastal flooding in Scituate (MA): A FVCOM study of the 818 27 December 2010 nor'easter. J. Geophys. Res. Ocean. 118, 6030–6045. 819 https://doi.org/10.1002/2013JC008862 820 Blankley, W.F., Lewin, R.A., 1976. Temperature responses of a coccolithophorid, Cricosphaera 821 carterae, measured in a simple and inexpensive thermal-gradient device. Limnol. 822 Oceanogr. 21. Bresnan, E., Fryer, R.J., Fraser, S., Smith, N., Stobo, L., Brown, N., Turrell, E., 2017. The 823 824 relationship between Pseudo-nitzschia (Peragallo) and domoic acid in Scottish shell fish. 825 Harmful Algae 63, 193-202. 826 Bresnan, E., Kraberg, A., Fraser, S., Brown, L., Hughes, S., Wiltshire, K.H., 2015. Diversity and 827 seasonality of Pseudo-nitzschia (Peragallo) at two North Sea time-series monitoring sites.

828	Helgol. Mar. Res. 69, 193–204. https://doi.org/10.1007/s10152-015-0428-5
829 830 831	Brickman, D., Hebert, D., Wang, Z., 2018. Mechanism for the recent ocean warming events on the Scotian Shelf of eastern Canada. Cont. Shelf Res. 156, 11–22. https://doi.org/10.1016/j.csr.2018.01.001
832 833	Brooks, D.A., 1987. The Influence of Warm-Core Rings on Slope Water Entering the Gulf of Maine. J. Geophys. Res. 92, 8183–8196.
834 835	Brooks, D.A., 1985. Vernal Circulation in the Gulf of Maine. J. Geophys. Reserach 90, 4687–4705.
836 837 838 839	Chen, C., Beardsley, R.C., Luettich, R.A., Westerink, J.J., Wang, H., Perrie, W., Xu, Q., Donahue, A.S., Qi, J., Lin, H., Zhao, L., Kerr, P.C., Meng, Y., Toulany, B., 2013. Extratropical storm inundation testbed: Intermodel comparisons in Scituate, Massachusetts. J. Geophys. Res. Ocean. 118, 5054–5073. https://doi.org/10.1002/jgrc.20397
840841842843	Churro, C.I., Carreira, C.C., Rodrigues, F.J., Craveiro, S.C., Calado, A.J., Casteleyn, G., Lundholm, N., 2009. Diversity and abundance of potentially toxic Pseudo-nitzschia peragallo in Aveiro Coastal Lagoon, Portugal and description of a new variety, P. pungens var. aveirensis var. nov. Diatom Res. 24, 35–62. https://doi.org/10.1080/0269249X.2009.9705782
844845846	Clark, S., Hubbard, K.A., Anderson, D.M., McGillicuddy, D.J.J., Ralston, D.K., Townsend, D.W., 2019. Pseudo-nitzschia bloom dynamics in the Gulf of Maine: 2012 – 2016. Harmful Algae 88, 101656. https://doi.org/10.1016/j.hal.2019.101656
847 848	Cummings, J.A., 2005. Operational multivariate ocean data assimilation. Q.J.R. Meterological Soc. 131, 3583–3604. https://doi.org/10.1256/qj.05.105
849 850 851	Cusack, C.K., Bates, S.S., Quilliam, M.A., Patching, J.W., Raine, R., 2002. Confirmation of domoic acid production by Pseudo-nitzschia australis (bacillariophyceae) isolated from Irish waters. J. Phycol 38, 1106–1112.
852 853 854	Dever, M., Hebert, D., Greenan, B.J.W., Sheng, J., Smith, P.C., 2016. Hydrography and Coastal Circulation along the Halifax Line and the Connections with the Gulf of St. Lawrence. Atmosphere-Ocean 54, 199–217. https://doi.org/10.1080/07055900.2016.1189397

855 Doucette, G.J., King, K.L., Thessen, A.E., Dortch, Q., 2008. The effect of salinity on domoic acid 856 production by the diatom Pseudo-nitzschia multiseries. Nov. Hedwigia 133, 31–46. 857 Ennaffah, B., Nafil, E., Chafik, A., 2012. First report of Pseudo-nitzschia australis on Moroccan 858 Atlantic coast and toxicity in Moroccan shellfish. Harmful Algae News 21. 859 Eppley, R.W., 1972. Temperature and phytoplankton growth in the sea. Fish. Bull. 70, 1063-860 1085. 861 Fehling, J., Davidson, K., Bolch, C., Tett, P., 2006. Seasonality of Pseudo-nitzschia 862 spp.(Bacillariophyceae) in western Scottish waters. Mar. Ecol. Prog. Ser. 323, 91–105. 863 Feldman, G.C., 2014. Diffuse attenuation coefficient for downwelling irradiance at 490 nm 864 [WWW Document]. URL https://oceancolor.gsfc.nasa.gov/atbd/kd_490/ (accessed 865 5.24.21). 866 Fennel, K., Wilkin, J., 2009. Quantifying biological carbon export for the northwest North 867 Atlantic continental shelves. Geophys. Res. Lett. 36, 2-5. 868 https://doi.org/10.1029/2009GL039818 869 Fernandes, L.F., Hubbard, K.A., Richlen, M.L., Smith, J., Bates, S.S., Ehrman, J., Léger, C., Mafra, 870 L.L., Kulis, D., Quilliam, M., Libera, K., McCauley, L., Anderson, D.M., 2014. Diversity and 871 toxicity of the diatom Pseudo-nitzschia Peragallo in the Gulf of Maine, Northwestern 872 Atlantic Ocean. Deep. Res. Part II Top. Stud. Oceanogr. 103, 139–162. 873 https://doi.org/10.1016/j.dsr2.2013.06.022 874 Hasle, G.R., 2002. Are most of the domoic acid-producing species of the diatom genus Pseudo-875 nitzschia cosmopolites? Harmful Algae 1, 137-146. https://doi.org/10.1016/S1568-876 9883(02)00014-8 877 He, R., McGillicuddy, D.J., Keafer, B.A., Anderson, D.M., 2008. Historic 2005 toxic bloom of 878 Alexandrium fundyense in the western Gulf of Maine: 2. Coupled biophysical numerical 879 modeling. J. Geophys. Res. Ocean. 113, 1–12. https://doi.org/10.1029/2007JC004602 880 Hebert, D., Pettipas, R., Brickman, D., Dever, M., 2018. Meteorological, Sea Ice and Physical 881 Oceanographic Conditions on the Scotian Shelf and in the Gulf of Maine during 2016.

882 Hubbard, K., Anderson, D., Archer, S., Berger, H., Brosnahan, M., Chadwick, C., Denny, E., 883 Disney, J., Farrell, A., Granholm, A., Fleiger, J., Flewelling, L., Heil, C., Henschen, K., Kanwit, 884 K., Kulis, D., Keafer, B., Keller Abbe, S., Lewis, B., Markley, L., Park, J., Petitpas, C., Racicot, 885 E., Robert, M., Villac, C., McGillicuddy, D., 2017. Synergistic characterization of Pseudo-886 nitzschia communities during unprecedented domoic acid events, in: Ninth Symposium on 887 Harmful Algae in the U.S. 888 Husson, B., Hernandez-Farinas, T., Le Gendre, R., Schapira, M., Chapelle, A., 2016. Two decades 889 of Pseudo-nitzschia spp. blooms and king scallop (Pecten maximus) contamination by 890 domoic acid along the French Atlantic and English Channel coasts: Seasonal dynamics, 891 spatial heterogeneity and interannual variability. Harmful Algae 51, 26–39. 892 https://doi.org/10.1016/J.HAL.2015.10.017 893 Interior, U.S.D. of the, 2021. USGS Water-Data Site Information for USA [WWW Document] URL 894 https://waterdata.usgs.gov/nwis (access 6.24.2021). 895 Klein, C., Claquin, P., Bouchart, V., Le Roy, B., Veron, B., 2010. Dynamics of Pseudo-nitzschia 896 spp. and domoic acid production in a macrotidal ecosystem of the Eastern English Channel 897 (Normandy, France). Harmful Algae 9, 218–226. https://doi.org/10.1016/J.HAL.2009.10.004 898 899 Lema, K.A., Latimier, M., Nézan, É., Fauchot, J., Le Gac, M., 2017. Inter and intra-specific growth 900 and domoic acid production in relation to nutrient ratios and concentrations in Pseudo-901 nitzschia: phosphate an important factor. Harmful Algae 64, 11–19. 902 https://doi.org/10.1016/j.hal.2017.03.001 903 Lewis, B., MacLeod, J., Hubbard, K., 2017. The Gulf of Maine domoic acid evento f 2016: an 904 emerging public health concern, in: 9th U.S. HAB Symposium. 905 Li, Y., He, R., 2014. Spatial and temporal variability of SST and ocean color in the Gulf of Maine 906 based on cloud-free SST and chlorophyll reconstructions in 2003-2012. Remote Sens. 907 Environ. 144, 98–108. https://doi.org/10.1016/j.rse.2014.01.019 908 Li, Y., He, R., Chen, K., McGillicuddy, D.J., 2015. Variational data assimilative modeling of the

909 Gulf of Maine in spring and summer 2010. J. Geophys. Res. Ocean. 132, 1–17. 910 https://doi.org/10.1002/2014JC010320.Received 911 Li, Y., He, R., McGillicuddy, D.J., Anderson, D.M., Keafer, B.A., 2009. Investigation of the 2006 912 Alexandrium fundyense bloom in the Gulf of Maine: In-situ observations and numerical 913 modeling. Cont. Shelf Res. 29, 2069–2082. https://doi.org/10.1016/j.csr.2009.07.012 914 Li, Y., Stumpf, R.P., McGillicuddy, D.J., He, R., 2020. Dynamics of an intense Alexandrium 915 catenella red tide in the Gulf of Maine: satellite observations and numerical modeling. 916 Harmful Algae 99, 101927. https://doi.org/10.1016/j.hal.2020.101927 917 López, A.G., Wilkin, J.L., Levin, J.C., 2020. Doppio-a ROMS (v3.6)-based circulation model for the 918 Mid-Atlantic Bight and Gulf of Maine: Configuration and comparison to integrated coastal 919 observing network observations. Geosci. Model Dev. 13, 3709–3729. 920 https://doi.org/10.5194/gmd-13-3709-2020 921 Lundholm, N., Clarke, A., Ellegaard, M., 2010. A 100-year record of changing Pseudo-nitzschia 922 species in a sill-fjord in Denmark related to nitrogen loading and temperature. Harmful 923 Algae 9, 449–457. https://doi.org/10.1016/j.hal.2010.03.001 924 Lynch, D.R., Holboke, M.J., Naimie, C.E., 1997. The Maine coastal current: Spring climatological 925 circulation. Cont. Shelf Res. 17, 605-634. https://doi.org/10.1016/S0278-4343(96)00055-6 926 McCabe, R.M., Hickey, B.M., Kudela, R.M., Lefebvre, K.A., Adams, N.G., Bill, B.D., Gulland, 927 F.M.D., Thomson, R.E., Cochlan, W.P., Trainer, V.L., 2016. An unprecedented coastwide 928 toxic algal bloom linked to anomalous ocean conditions. Geophys. Res. Lett. 43, 10,366-929 10,376. https://doi.org/10.1002/2016GL070023 930 McGillicuddy, D.J., Brosnahan, M.L., Couture, D.A., He, R., Keafer, B.A., Manning, J.P., Martin, 931 J.L., Pilskaln, C.H., Townsend, D.W., Anderson, D.M., 2014. A red tide of Alexandrium 932 fundyense in the Gulf of Maine. Deep. Res. Part II Top. Stud. Oceanogr. 103, 174–184. 933 https://doi.org/10.1016/j.dsr2.2013.05.011 934 McGillicuddy, D.J.J., Townsend, D.W., He, R., Keafer, B.A., Kleindinst, J.L., Li, Y., Manning, J.P., 935 Mountain, D.G., Thomas, M.A., Anderson, D.M., 2011. Suppression of the 2010

936 Alexandrium fundyense bloom by changes in physical, biological, and chemical properties 937 of the Gulf of Maine. Limnol. Oceanogr. 56, 2411-2426. 938 https://doi.org/10.4319/lo.2011.56.6.2411 939 Mesinger, F., DiMego, G., Kalnay, E., Mitchell, K., 2006. North American Regional Reanalysis. 940 Bull. Am. Meteorol. Soc. 87, 343-360. https://doi.org/10.1175/BAMS-87-3-343 941 Morse, R.E., Friedland, K.D., Tommasi, D., Stock, C., Nye, J., 2017. Distinct zooplankton regime 942 shift patterns across ecoregions of the U.S. Northeast continental shelf Large Marine 943 Ecosystem. J. Mar. Syst. 165, 77–91. https://doi.org/10.1016/j.jmarsys.2016.09.011 944 Norberg, J., 2004. Biodiversity and ecosystem functioning: A complex adaptive systems 945 approach. Limnol. Oceanogr. 49, 1269–1277. 946 https://doi.org/10.4319/lo.2004.49.4 part 2.1269 947 North, E.W., Hood, R.R., Chao, S.-Y., Sanford, L.P., 2006. Using a random displacement model to 948 simulate turbulent particle motion in a baroclinic frontal zone: A new implementation 949 scheme and model performance tests. J. Mar. Syst. 60, 365–380. 950 https://doi.org/10.1016/j.jmarsys.2005.08.003 951 North, E.W., Schlag, Z., Hood, R.R., Li, M., Zhong, L., Gross, T., Kennedy, V.S., 2008. Vertical 952 swimming behavior influences the dispersal of simulated oyster larvae in a coupled 953 particle-tracking and hydrodynamic model of Chesapeake Bay. Mar. Ecol. Prog. Ser. 359, 954 99–115. https://doi.org/10.3354/meps07317 955 Ohashi, K., Sheng, J., 2013. Influence of St. Lawrence River discharge on the circulation and 956 hydrography in Canadian Atlantic waters. Cont. Shelf Res. 58, 32–49. 957 https://doi.org/10.1016/j.csr.2013.03.005 958 Palma, S., Mouriño, H., Silva, A., Barão, M.I., Moita, M.T., 2010. Can Pseudo-nitzschia blooms be 959 modeled by coastal upwelling in Lisbon Bay? Harmful Algae 9, 294-303. 960 https://doi.org/10.1016/j.hal.2009.11.006 961 Pershing, A.J., Alexander, M.A., Hernandez, C.M., Kerr, L.A., Le Bris, A., Mills, K.E., Nye, J.A., 962 Record, N.R., Scannell, H.A., Scott, J.D., Sherwood, G.D., Thomas, A.C., 2015. Slow

963 adaptation in the face of rapid warming leads to collapse of the Gulf of Maine cod fishery. 964 Science (80-.). 350, 809–812. https://doi.org/10.1126/science.aac9819 965 Pershing, A.J., Mills, K.E., Dayton, A.M., Franklin, B.S., Kennedy, B.T., 2018. Evidence for 966 adaptation from the 2016 marine heatwave in the Northwest Atlantic Ocean. 967 Oceanography 31. https://doi.org/https://doi.org/10.5670/oceanog.2018.213 968 Pettigrew, N.R., Churchill, J.H., Janzen, C.D., Mangum, L.J., Signell, R.P., Thomas, A.C., 969 Townsend, D.W., Wallinga, J.P., Xue, H., 2005. The kinematic and hydrographic structure of 970 the Gulf of Maine Coastal Current. Deep. Res. Part II Top. Stud. Oceanogr. 52, 2369–2391. 971 https://doi.org/10.1016/j.dsr2.2005.06.033 972 Ryan, J.P., Kudela, R.M., Birch, J.M., Blum, M., Bowers, H.A., Chavez, F.P., Doucette, G.J., 973 Hayashi, K., Marin, R., Mikulski, C.M., Pennington, J.T., Scholin, C.A., Smith, G.J., Woods, A., 974 Zhang, Y., 2017. Causality of an extreme harmful algal bloom in Monterey Bay, California, 975 during the 2014–2016 northeast Pacific warm anomaly. Geophys. Res. Lett. 44, 5571– 976 5579. https://doi.org/10.1002/2017GL072637 977 Schlag, Z.R., North, E.W., 2012. Lagrangian TRANSport model User's Guide. 978 Shchepetkin, A.., McWilliams, J.C., 2005. The regional oceanic modeling system (ROMS): A split-979 explicit, free-surface, topography-following-coordinate oceanic model. Ocean Model. 9, 980 347-404. 981 Simons, R.D., Siegel, D.A., Brown, K.S., 2013. Model sensitivity and robustness in the estimation 982 of larval transport: A study of particle tracking parameters. J. Mar. Syst. 119–120, 19–29. 983 https://doi.org/10.1016/j.jmarsys.2013.03.004 984 Smith, P.C., Pettigrew, N.R., Yeats, P., Townsend, D.W., Han, G., 2012. Regime Shift in the Gulf 985 of Maine. Am. Fish. Soc. Symp. 79, 185-203. Thessen, A.E., Dortch, Q., Parsons, M.L., Morrison, W., 2005. Effect of salinity on Pseudo-986 987 nitzschia species (Bacillariophyceae) growth and distribution. J. Phycol. 41, 21–29. 988 https://doi.org/10.1111/j.1529-8817.2005.04077.x

Thessen, A.E., Stoecker, D.K., 2008. Distribution, abundance and domoic acid analysis of the

990 toxic diatom genus Pseudo-nitzschia from the Chesapeake Bay. Estuaries and Coasts 31, 991 664-672. https://doi.org/10.1007/s12237-008-9053-8 992 Thomas, M.K., Kremer, C.T., Klausmeier, C.A., Litchman, E., 2012. A global pattern of thermal 993 adaptation in marine phytoplankton. Science (80-.). 338, 1085–1088. 994 https://doi.org/10.1126/science.1224836 995 Thorel, M., Claquin, P., Schapira, M., Le Gendre, R., Riou, P., Goux, D., Le Roy, B., Raimbault, V., 996 Deton-Cabanillas, A.F., Bazin, P., Kientz-Bouchart, V., Fauchot, J., 2017. Nutrient ratios 997 influence variability in Pseudo-nitzschia species diversity and particulate domoic acid 998 production in the Bay of Seine (France). Harmful Algae 68, 192–205. 999 https://doi.org/10.1016/j.hal.2017.07.005 1000 Thorel, M., Fauchot, J., Morelle, J., Raimbault, V., Le Roy, B., Miossec, C., Kientz-Bouchart, V., 1001 Claquin, P., 2014. Interactive effects of irradiance and temperature on growth and domoic 1002 acid production of the toxic diatom Pseudo-nitzschia australis (Bacillariophyceae). Harmful 1003 Algae 39, 232–241. https://doi.org/10.1016/j.hal.2014.07.010 1004 Townsend, D.W., Pettigrew, N.R., Thomas, M.A., Neary, M.G., Mcgillicuddy, D.J., Donnell, J.O., 1005 2015. Water masses and nutrient sources to the Gulf of Maine. J. Mar. Res. 141, 93–122. 1006 https://doi.org/10.1038/141548c0 1007 Townsend, D.W., Rebuck, N.D., Thomas, M.A., Karp-Boss, L., Gettings, R.M., 2010. A changing 1008 nutrient regime in the Gulf of Maine. Cont. Shelf Res. 30, 820–832. 1009 https://doi.org/10.1016/j.csr.2010.01.019 1010 Townsend, D.W., Thomas, A.C., Mayer, L.M., Thomas, M.A., Quinlan, J.A., 2006. Oceanography of the Northwest Atlantic Shelf (1, W), in: The Sea: The Global Coastal Ocean: 1011 1012 Interdisciplinary Regional Studies and Syntheses. Harvard University Press, pp. 119–168. 1013 Trainer, V.L., Bates, S.S., Lundholm, N., Thessen, A.E., Cochlan, W.P., Adams, N.G., Trick, C.G., 1014 2012. Pseudo-nitzschia physiological ecology, phylogeny, toxicity, monitoring and impacts 1015 on ecosystem health. Harmful Algae 14, 271-300. 1016 https://doi.org/10.1016/j.hal.2011.10.025

1017	Trainer, V.L., Moore, S.K., Hallegraeff, G., Kudela, R.M., Clement, A., Mardones, J.I., Cochlan,
1018	W.P., 2020. Pelagic harmful algal blooms and climate change: Lessons from nature's
1019	experiments with extremes. Harmful Algae 91, 101591.
1020	https://doi.org/10.1016/j.hal.2019.03.009
1021	Wallcraft, A., Carroll, S.N., Kelly, K.A., Rushing, K.V., 2003. Hybrid Coordinate Ocean Model
1022	(HYCOM) User's Guide, Version 2.1.
1023	Xue, H., Chai, F., Pettigrew, N.R., 2000. A Model Study of the Seasonal Circulation in the Gulf of
1024	Maine. J. Phys. Oceanogr. 30, 1111–1135. https://doi.org/10.1175/1520-
1025	0485(2000)030<1111:AMSOTS>2.0.CO;2
1026	Zapata, M., Rodriguez, F., Fraga, S., Barra, L., Ruggiero, M.V., 2011. Chlorophyll C pigment
1027	patterns in 18 species (51 strains) of the genus Pseudo-nitzschia (bacillariophyceae). J.
1028	Phycol 47, 1274–1280. https://doi.org/10.1111/j.1529-8817.2011.01055.x
1029	